

# A-type Supergiant Abundances in the SMC: Probes of Evolution

Kim A. Venn<sup>1</sup>

Macalester College

Received \_\_\_\_\_; accepted \_\_\_\_\_

arXiv:astro-ph/9901306v1 21 Jan 1999

---

<sup>1</sup>Postdoctoral work while at Universität Sternwarte München, Scheinerstrasse 1, D-81679, Munich, Germany, and Max-Planck-Institut für Astrophysik Karl-Schwarzschildstr. 2, 85740 Garching, Germany

## ABSTRACT

New abundances of N, O, Na, Mg, Si, Ca, Sc, Ti, Cr, Fe, Sr, Zr, and Ba are presented for 10 A-type supergiants in the SMC, plus upper limits for C. In interpreting the CNO results for constraints on stellar evolution theories, careful attention has been paid to the comparison abundances, i.e., the present day abundances of SMC nebulae and B-dwarf stars. These new results are also compared to published results from F-K supergiant analyses, and found to be in good agreement when both sets of data are carefully examined as differential (SMC minus Galactic standard) abundances.

With the exception of nitrogen, very small star-to-star abundance variations are found for all elements in this analysis. The N variations are *not* predicted by standard stellar evolution models. Instead, the results support the new predictions reported from rotating stellar models, where the range in nitrogen is the result of partial mixing of CN-cycled gas from the stellar interior due to main-sequence rotation at different rates (c.f., Langer & Heger 1998). The overall overabundance of nitrogen in the sampled stars also implies these stars have undergone the first dredge-up in addition to having been mixed while on the main-sequence.

The alpha-elements (O, Mg, Si, Ca, Ti) have similar underabundances to Fe, which is not the same as seen in metal-poor stars in the solar neighborhood of the Galaxy. In addition, certain light s-process elements (Zr, Ba) are slightly more underabundant than Fe, which is predicted by the bursting chemical evolution model presented by Pagel & Tautvaišienė (1998) for the SMC.

*Subject headings:* stars: abundances – stars: atmospheres – stars: evolution – supergiants – Small Magellanic Cloud

## 1. Introduction

Abundance analyses of supergiants in the Small Magellanic Cloud (SMC) have several applications. In particular, they can be used to study metallicity effects on the evolution of massive stars, and they yield information on the present-day chemical composition of the SMC, which is an important constraint on SMC evolution models.

The A-type supergiants have proved to be very useful abundance indicators based on the tailored analyses of 22 Galactic stars by Venn (1995a,b). In fact, the accuracy of the elemental abundances from a tailored analysis (see Section 3 for details) certainly rivals that from any other supergiant analysis, e.g., F-K supergiants. In A-type supergiant atmospheres, it is now known that NLTE effects are often *less* significant on the model atmosphere structure (temperature and pressure versus optical depth) than line blanketing effects (Przybilla 1997, also see Section 3.1 for a demonstration using H $\gamma$  line profiles). In addition, the spectra of A-type supergiants are very clean (unlike the more crowded spectra of F-K supergiants), with many unblended, important spectral features that are ideal abundance indicators.

A-type supergiants are also known to be the brightest stars at visual wavelengths, which makes them ideal targets for extragalactic stellar analyses. It is possible to observe features from a wide variety of elements in their spectra, ranging from light elements (B, CNO) to s-process elements (Sr, Zr, Ba). These can be used to study abundance gradients or element abundance dispersions in Local Group galaxies (e.g., McCarthy et al. 1995, Venn et al. 1998). In the SMC, elemental abundances from F-K supergiants (Luck et al. 1998, Hill et al. 1997a,b, Luck & Lambert 1992, Spite et al. 1989a,b, Russell & Bessell 1989), planetary nebulae (c.f., Dopita et al. 1997), supernovae remnants (c.f., Russell & Dopita 1990), and H II regions (Dufour 1984, Russell & Dopita 1990, Garnett et al. 1995, Kurt et al. 1998) have shown that  $\alpha$ -elements share the underabundance of iron-group elements. This is

interesting because metal-poor stars in the Galaxy tend to have higher abundances of  $\alpha$  elements (c.f., Edvardsson et al. 1993) due to early enrichments from Type II supernovae (c.f., Pagel & Tautvaišienė 1995). Various SMC evolution scenarios have been proposed to account for these observations (e.g., Pagel & Tautvaišienė 1998, Tsujimoto et al. 1995, Russell & Dopita 1992). The abundances available from the A-type supergiants nicely complement those in the literature for these studies.

That A-supergiants are evolved massive stars also means that the light element abundances can be used to study stellar evolution effects. In the Galaxy, most supergiants show evidence for some mixing of CNO-cycled gas at their surfaces (e.g., Gies & Lambert 1992, Lennon 1994, Venn 1995a, Luck & Lambert 1985, Spite & Spite 1990, Boyarchuk et al. 1985), an observation that most stellar evolution scenarios fail to predict. Additionally, some main-sequence B stars show enhanced N (Gies & Lambert 1992), which strongly suggests that slight mixing can occur on the main-sequence in a small number of massive stars. New massive star evolution calculations that include rotation effects do predict some mixing between the stellar layers which can cause slight changes in the surface abundances (e.g., Langer & Heger 1998, Talon et al. 1998, Maeder & Zahn 1998, Meynet 1997, Fliegner et al. 1996, Denissenkov 1994). The extent of mixing depends on several parameters, e.g., rotation rate and mass, but the success of mixing can also depend on convection parameters, mass loss rate, and metallicity. The effects of rotation on stellar evolution calculations may have far reaching consequences, e.g., the evolution track for a rapidly-rotating  $10 M_{\odot}$  star can intersect that of a slowly-rotating  $20 M_{\odot}$  star in the blue supergiant region (see Fig. 2 in Fliegner et al. 1996). Such a change in evolution tracks could have a great impact on all uses of stellar evolution models, including mass and age estimates of young stars and clusters and population syntheses of star-forming regions and galaxies. The Magellanic Clouds provide an ideal laboratory to study the metallicity effects of these new stellar evolution models.

In this paper, new atmospheric parameters and elemental abundances are determined for 10 SMC A-type supergiants. The results are used to examine metallicity effects on stellar evolution through comparisons with Galactic A-type supergiants (to reduce systematic errors) and comparisons with SMC nebular and B-dwarf abundances. In addition, the abundances provide new data to constrain chemical evolution models of the SMC, the closest and best studied of all metal-poor dwarf irregular galaxies.

## 2. Observations

Spectral data were taken during two observing runs at the European Southern Observatory in September and November 1995 at the 3.6 m telescope. CASPEC ( $R \sim 30,000$ ) was used in two wavelength regions, providing full wavelength coverage from 3900 to 8300 Å, with only a small gap from 5300 to 5900 Å. The S/N ranged from 70 to 120 per resolution element, and rapidly-rotating hot stars with similar air masses to the SMC were observed at red wavelengths to remove telluric lines. Standard IRAF<sup>2</sup> packages were used for the data reduction (for more details see Venn 1993).

Program stars were chosen from the Azzopardi & Vigneau (1982) catalogue of SMC bright stars. This catalogue provided positions, visual magnitudes, colors, and spectral types with luminosity classes. An attempt has been made to observe A-supergiants over a range of luminosities, thus masses, especially for comparison with the Galactic stars; see Fig. 1. Furthermore, lower luminosity A-type supergiants (e.g., with luminosity classes Ib) are not expected to suffer significantly from microvariability, stellar wind effects, or

---

<sup>2</sup>IRAF is distributed by the National Optical Astronomy Observatories which is operated by the Association of Universities for Research in Astronomy, Inc., under cooperative agreement with the National Science Foundation.

departures from LTE (for lines that form deep in the photosphere). Therefore, analysis of those stars should yield the most reliable abundance results, although in the SMC (see below) as in the Galaxy (Venn 1995 a,b), no significant differences in abundances have been seen between the Ia and Ib supergiants.

### 3. Atmospheric Analysis

Kurucz ATLAS9 (1979, 1991) model atmospheres have been adopted throughout. The assumptions of LTE and plane-parallel geometry for the model structure have been shown to be satisfactory for A-type supergiants in a *tailored* analysis, i.e., when only weak lines that form deep in the atmosphere are used (see the discussion by Venn 1995b). The important advantage of the ATLAS9 models is the extensive metal line blanketing which has a significant effect on the temperature structure of A-type supergiants.

As an example, an investigation of the effects of NLTE on the  $H\gamma$  line in A-supergiant model atmospheres shows that the results from the ATLAS9 LTE models are very similar to those from the Kunze NLTE models (Kudritzki, private communications) at low gravities. In Fig.2,  $H\gamma$  line profiles are shown based on ATLAS9 models (with extensive line blanketing via an opacity distribution function, ODF), ATLAS8 models (no line blanketing, H and He bound-free edges only), and Kunze NLTE models (no line blanketing, H and He bound-free edges only). At the lowest gravities, all three profiles are very similar, e.g., at  $T_{\text{eff}}=8800$  K and  $\log g=1.1$ , (see Fig. 2, left panel). Thus, NLTE and line blanketing are equally unimportant! At higher gravities, the profiles do not agree as well, yet we expect the Kurucz models to be better since NLTE effects *decrease* with increasing gravity and line blanketing effects remain important. Thus, Kurucz ATLAS9 line-blanketed model atmospheres are the best available for A-supergiant abundance analyses at present.

In addition, Kaufer et al. (1996) have shown that some very luminous A-supergiants have strongly variable Balmer lines, which would be a problem for this analysis. However, this variability is predicted to be due to changes in a stellar wind, and does not appear to affect the photospheric absorption lines, including the extended  $H\gamma$  line wings.

### 3.1. Atmospheric Parameters

The atmospheric parameters determined for the SMC A-type supergiants are listed in Table 1. The “new” spectral types are based on the atmospheric parameters as listed in Table 1 (“old” spectral types are those listed by Azzopardi & Vigneanu 1982). These stars were analysed using the same methods as Venn (1995a,b).

Atmospheric parameters were determined from the intersection point of two spectroscopic parameters that are sensitive to both temperature and gravity. One indicator is the wing profile of the  $H\gamma$  (and often  $H\delta$ ) Balmer line. Sample profile fits are shown in Fig. 3. The wings of the Balmer lines form deep in the atmosphere where uncertainties due to recombination in a stellar wind or extended envelope and microvariability effects can be ignored. The other is the locus of parameters that yield  $\log(\text{Mg I}/\text{H})=\log(\text{Mg II}/\text{H})$  (and where the Mg abundance itself is not fixed). Sample spectra of some Mg I and Mg II absorption lines are shown in Fig. 4. The accuracies in the atmospheric parameters resulting from these spectral indicators are listed in Table 2.

If only weak lines of Mg I and Mg II are used, that form deep in the photosphere, then NLTE effects on the line formation are small. Calculations show that NLTE corrections are typically less than 0.1 dex throughout when the line strengths are less than about 100  $m\text{\AA}$  (using the detailed Mg I/II model atom by Gigas 1988, and analysis methods by Venn 1995b). NLTE corrections have been included here when determining the atmospheric

parameters, even though the corrections are small (typically +0.1 dex for Mg I and –0.1 dex for Mg II for weak lines only). Estimates of the systematic offsets if NLTE is not considered are shown in Table 2.

Takeda (1994) has commented that strong Mg lines may not be good atmospheric parameter indicators if there is a contribution from an extended atmosphere, which would affect the line symmetry. There is no evidence for line asymmetries in the weak Mg lines used (here and for the Galactic stars). Furthermore, these lines have high excitation potentials, thus forming deep in the photosphere, where any wind or chromospheric component would be negligible.

Microturbulence values in Table 1 have been determined from ionized species of Fe, Ti and Cr, when enough lines over a variety of line strengths are present. There is some evidence for slightly different values for each species, particularly between neutral and ionized species of the same element (e.g., Fe I and Fe II). These differences are typically small though ( $\pm 1\text{--}3 \text{ km s}^{-1}$ ), and the weak lines analysed herein are not very sensitive to the  $\xi$  value. Thus, a single value that best fits all species has been adopted per star, with  $\Delta\xi = \pm 1 \text{ km s}^{-1}$ . Radial and rotational velocities in Table 1 have been determined from spectrum synthesis of Fe II and O I lines near  $6150 \text{ \AA}$ ;  $\Delta v_{\text{rad}}$  and  $\Delta v \sin i = \pm 5 \text{ km s}^{-1}$ .

### 3.2. Spectral Types and Atmospheric Parameters

Examinations of blue supergiants in the Magellanic Clouds have shown that the spectral types assigned to these stars are often incorrect (Fitzpatrick 1991, Lennon 1997). This is because the classical MK classification system cannot be easily applied to metal-poor stars. A typical mistake is to give a metal-poor B-type star a spectral type that is too hot because the metal lines are weaker in both cases. In response to this, Fitzpatrick (1991)



presented a new classification scheme for LMC B-type supergiants, and Lennon (1997) has done the same for the SMC. It is striking to see the differences in stars of the same spectral type due to metallicity alone (compare Lennon’s Fig. 5 of Galactic stars to his Fig. 6 for SMC stars).

The same is found in this analysis of SMC A-supergiants. Almost all of the A-type supergiants are cooler than their previously assigned spectral types would indicate; see Table 1. Some stars are also less luminous than had been previously indicated from their luminosity classes. This is an important point since some A-supergiants in the SMC were reported to have “anomalous” spectral features such as Balmer lines that are too strong for their luminosity classes and the UBV colors that are too blue (Humphreys 1983, Humphreys et al. 1991). It had been proposed that these anomalies were due to an enrichment of helium in the stellar atmospheres, however the anomalies are eliminated once the cooler temperatures and lower luminosities determined here are adopted. All of the “anomalous” A-supergiants in this analysis have cooler temperatures, e.g., AV 254 and AV 478 were reported as anomalous A3 Ia stars (Humphreys 1983, Humphreys et al. 1991), whereas the atmospheric parameters are like normal A7 Iab stars. Oddly, a nearly identical A7 Iab star, AV 442, was classified as a normal A3 Ia star (Ardeberg & Maurice 1977). The  $H\gamma$  spectra of these three stars are shown together in Fig. 5, which clearly shows they are nearly identical. Ironically, the “anomalous A3 Ib” star AV 392 appears to be the only properly classified star, A3 Ib, except that it is normal.

Star AV 213 was also clearly misclassified, or it has changed its spectral type (an LBV star?). This star is definitely not a normal A2 Iab star (Azzopardi & Vigneau 1982, Humphreys 1983) as the  $H\alpha$  profile is in emission (unlike the other supergiants) and the metal lines are stronger than most of the other stars. The atmospheric parameters are typical of a high luminosity F0 Ia hypergiant. In addition, the metal abundances of this

star are consistent to within 0.2 dex, just like the other A-supergiants analysed which implies the atmospheric analysis is rather robust.

Finally, the atmospheric parameters for two stars, AV 110 and AV 174 (the hottest and coolest stars in the sample), are slightly more uncertain than most since only one line of Mg I and/or Mg II was available.

#### 4. Elemental Abundances

The chemical abundances in each star have been calculated assuming the best available atomic data in the literature (see the discussions in Venn 1995a,b, and references in Appendix A). Individual stellar abundances and estimated uncertainties are listed in Tables 3–6 as  $12+\log(X/H) \pm \sigma$  ( $\#$ ), where  $\#$  is the number of lines used in the average (“S” in the LTE O I row refers to spectrum synthesis). In three cases, N, O, and Mg, both LTE (italicized) and NLTE corrected abundances are listed; the LTE abundances are only shown for comparison. Note that the NLTE corrections are calculated for the line formation of those three individual elements only within an LTE ATLAS9 model atmosphere (discussed previously as the best models for A-type supergiants in Section 3). Individual spectral line data is listed in Appendix A.

Mean abundances for the sample are listed in Table 7, including the Galactic A-supergiant results and solar abundances (from Anders & Grevesse, 1989, and Grevesse & Noels, 1993) for comparison. These abundances are also graphed in Fig. 6 as unweighted averages of all the stars analysed relative to Galactic A-supergiant abundances. Most elemental abundances determined previously for Galactic A-type supergiants are similar to solar (or to the solar neighborhood in the case of CNO), a result which was used to emphasize the success of the tailored atmospheric analysis of these otherwise complex stars.

*Carbon upper limits:* Upper limits can be placed on the C abundances, through non-detections of the most accurate C I indicator, i.e., the  $\lambda\lambda 7115$  multiplet. Adopting  $15 \text{ m}\text{\AA}$  as a limiting equivalent width (which is approximately  $1\text{-}\sigma$  in the S/N of the spectra) then the upper limits for the cooler stars are intriguing,  $[\text{C}/\text{H}] \leq -1.3$  for AV 174. This is consistent with the value for C derived from the H II region observations (see Section 6.1). NLTE corrections could lower the C limits further (by  $\leq 0.3$  dex, based on calculations using the Stürenburg & Holweger 1990 C I/II model atom). These corrections put the upper limits for the six coolest stars in this analysis in agreement with the nebular/B-star abundances.

*Nitrogen:* Nitrogen abundances have been determined from the spectral lines of two N I multiplets,  $\lambda\lambda 7440$  and  $\lambda\lambda 8210$ . Sample spectra are shown in Fig. 7. Both multiplets include lines of various strengths that are uncontaminated by other elemental features (except telluric lines which are removed by a hot standard star observed near the same airmass). The LTE nitrogen abundances are near solar, with only a few exceptions (see Tables 3 and 5), although NLTE effects are significant.

In the Galaxy, NLTE corrections range from  $-1.0$  dex in A0 supergiants to  $-0.3$  dex by the F0. NLTE corrections also remove a trend in N with effective temperature and line strength. Using the same N I/II model atom and techniques as for the Galactic stars, NLTE corrections have been computed for the nitrogen abundances in the SMC stars. The lower metallicity of these stars has a negligible effect on the statistical equilibrium of N I relative to their Galactic counterparts. As discussed by Lemke & Venn (1996), this is because the statistical equilibrium is almost completely controlled by the UV flux around  $1200 \text{ \AA}$  through the photoionization of the N I  $2p^2P^0$  ground state. This spectral region is dominated primarily by C I bound-free transitions and H I  $\text{Ly}\alpha$  absorption. Therefore, uncertainties in the NLTE corrections for N I in the SMC stars are similar to those reported

by Venn (1995a, Table 7 therein) for Galactic stars, i.e., typically  $\leq \pm 0.1$  dex.

The only remaining tricky part for the N I NLTE calculations for the SMC stars is adopting a carbon abundance. Since C could not be determined for each star in this analysis,  $\log(\text{C}/\text{H})+12=7.3$  was adopted for the calculations. This value is indicated by the nebular abundances, it is supported by the main-sequence SMC B-stars, and corresponds to the upper limit on the A-supergiant, AV 174, in this analysis. If the carbon abundance is reduced to  $\log(\text{C}/\text{H})+12=7.0$ , e.g., if mixing of CN-cycled gas has occurred which would reduce C at the stellar surface, then the NLTE N I corrections are not strongly affected (the corrections are larger by  $\leq 0.03$  dex). If C is higher, e.g.,  $\log(\text{C}/\text{H})+12=7.6$ , then the NLTE corrections can be slightly smaller, i.e., NLTE N abundances could be  $\sim 0.05$  dex higher.

The mean NLTE nitrogen abundance of 9 A-supergiants in this analysis is  $\log(\text{N}/\text{H})+12=7.33 \pm 0.35$ . The scatter in the abundances is quite large; larger than is expected from only atmospheric analysis uncertainties. In particular, in two cases, stars with very similar atmospheric parameters have the largest differences in N, i.e.,  $\text{N}(\text{AV 213}) = \text{N}(\text{AV 174}) + 1.0$ , and  $\text{N}(\text{AV 478}) = \text{N}(\text{AV 254}) + 0.5$ . This alone argues that the star to star variations seen in the N abundances are real. In addition, the range in the abundances of other elements from star-to-star are quite small (see Table 7 and Fig. 6, discussed further in Section 6.2).

*Oxygen:* O I is determined from spectrum synthesis of the  $\lambda\lambda 6158$  multiplet throughout (see Fig. 8 for samples of the spectra), plus the  $\lambda 6454$  line in AV 442. The multiplet comprises three weak lines that are free of blends in this temperature regime. Uncertainties in  $v \sin i$  and the S/N of the spectra dominate the small LTE oxygen abundance uncertainties, which are listed in Tables 4 & 6.

NLTE corrections to these oxygen abundances can be estimated based on the detailed calculations of O I in A-F stars by Baschek et al. (1977) and Takeda (1992). Baschek

et al. use the complete linearization method and build a simple 8 level model atom with only 7 explicit line transitions. Assuming theoretical photoionization and collisional rates, they determine NLTE corrections for various multiplets in modified Kurucz (1969) model atmospheres (without line blanketing). They report a reduction in the theoretical equivalent widths for the O I  $\lambda\lambda 6158$  multiplet lines by 65%/15% for models at 10000 K/7500 K with  $\log g=1.0$ . In this analysis, these translate to abundance corrections of  $-0.5/-0.15$  dex.

On the other hand, Takeda (1992) uses the ALI (accelerated-lambda-iteration) method and builds a model atom with 86 levels and 294 explicit line transitions. Adopting different photoionization rates than Baschek et al. (hydrogenic versus scaled Thomas-Fermi values), and updating the oscillator strengths, Takeda determines the NLTE corrections for various multiplets in newer Kurucz (1979) line blanketed model atmospheres (e.g., at 9500 K and 6500 K, with  $\log g=1.5$ ). Remarkably, Takeda’s NLTE corrections for the  $\lambda\lambda 6158$  lines are almost identical to Baschek et al.’s. Oxygen from  $\lambda\lambda 6158$  in the hotter/cooler supergiants is reduced by  $-0.35/-0.1$  dex.

In this paper, these NLTE corrections for the oxygen abundances in A-F supergiants have been adopted, scaling the corrections to reflect temperature and luminosity differences, as follows;

$$\Delta\text{O I } (T_{\text{eff}} \geq 9000 \text{ K}) = -0.3,$$

$$\Delta\text{O I } (8500 > T_{\text{eff}} \geq 8000 \text{ K and } \log g > 1.5) = -0.2,$$

$$\Delta\text{O I } (8500 > T_{\text{eff}} \geq 8000 \text{ K and } \log g \leq 1.5) = -0.1,$$

$$\Delta\text{O I } (T_{\text{eff}} < 8000 \text{ K}) = -0.1 \text{ (see Tables 3 \& 5).}$$

The mean NLTE corrected oxygen abundance is then  $\log(\text{O}/\text{H})+12=8.14$ . Retaining the uncertainty from the LTE spectrum syntheses (which should continue to dominate the abundance uncertainties), then  $[\text{O I}/\text{Fe II}]=0.00 \pm 0.10$ . Oxygen, however, is higher in the

Sun than in other objects in the solar neighborhood, including Galactic A-supergiants. Adopting the same NLTE corrections for the Galactic A-supergiant abundances in Venn (1995a), then NLTE  $O(\text{GAL AI's}) = 8.59$ . Thus, the differential abundance is  $-0.45$  dex (i.e.,  $\log(O/H)_{\text{SMC}} - \log(O/H)_{\text{GAL AI}}$ ).

Adopting the same NLTE corrections for the Galactic A-supergiants assumes that there is no significant metallicity dependence to them. This is not a bad assumption considering that Takeda and Baschek et al. derived very similar results using different initial O abundances ( $12 + \log(O/H) = 8.8$  and  $8.6$ , respectively) and different model atmospheres (e.g., Takeda's included line blanketing).

Thus, the differential O underabundance,  $-0.45$  dex, is slightly smaller than the iron underabundance,  $-0.6$  dex, but it is in good agreement with the differential O abundance from nebulae and B-stars, e.g.,  $-0.5$  dex (discussed in Section 6.1).

*Sodium:* Na has been determined from the Na D resonance lines, and/or Na I (mult. #4) at  $\lambda 8194$  in six stars. Sodium abundances range from being in good agreement with the iron-group underabundances, to showing slight enhancements. The average of this sample is  $[\text{Na I}/\text{Fe II}] = +0.23 \pm 0.2$ .

A large overabundance of Na was seen in the Galactic A-type supergiants from the same spectral features,  $[\text{Na}/\text{H}] = +0.66$ . Overabundances of Na have also been found in Galactic F-K supergiants and interpreted in a number of ways (see the review by Lambert 1992). NLTE effects have been ruled out by Drake & Lambert (1994), but other failures of the model atmospheres analyses may still exist. In the SMC, it is also unclear as to what the initial Na abundance should be in young stars, making any interpretation based on stellar surface changes difficult.

*Iron-group:* Fe II, Cr II, and Ti II are determined from several lines throughout the

optical spectra, and from a variety of multiplets with different line strengths and excitation potentials. The mean of these abundances is  $[M/H] = -0.7 \pm 0.2$  (or  $-0.6$  dex relative to Galactic A-supergiants). Uncertainties in the atmospheric parameters have only small effects on these abundances ( $\Delta(\text{Fe II}, \text{Cr II}) \leq \pm 0.14$  dex,  $\Delta(\text{Ti II}) \leq \pm 0.2$  dex).

Fe I is measured from many weak lines, and is typically 0.0 to 0.3 dex lower than Fe II. This is consistent with the underabundances predicted from NLTE calculations in Galactic A-dwarfs (Gigas 1986) and early-F supergiants (Boyarchuk et al. 1985). NLTE effects cause Fe I to be overionized by the UV radiation field, which one might expect to be affected by metallicity through line blanketing, although Gigas (1986) examined metallicity effects in Vega ( $[\text{Fe}/\text{H}] = 0$  and  $-0.5$ ), and found negligible differences in the NLTE corrections.

Sc II is consistent with the iron-group results, although measured from far fewer lines. Additionally, Cr I is determined in three stars (AV 463, 213, and 174, from 2-3 lines of multiplet #7 near  $\lambda 5206$ ), and is in good agreement with Cr II throughout.

*Alpha-elements:* Mg, Si, and Ca (Ti is discussed above with the iron-group elements) are primarily synthesized together during explosive O and Si burning through the addition of  $\alpha$  particles to lighter seed nuclei. Most of the  $\alpha$ -element underabundances determined here are in excellent agreement with the iron-group underabundances.

Magnesium, determined from weak and unblended Mg I and Mg II lines (that have been critically tested for accuracy, see Venn 1995b) is always consistent with the iron-group underabundance (to within  $1\sigma$ ). Uncertainties in the atmospheric parameters hardly affect Mg II, making it an excellent abundance indicator in this temperature regime.

Silicon abundances are measured from 2 to 6 lines of Si II in all the target stars. In most stars, the silicon depletion is the same as the iron-group and Mg depletions to within 0.2 dex. Some of the hotter stars appear to be slightly overabundant,  $[\text{Si}/\text{Fe}] \geq 0.3$ , which

may suggest an increasing NLTE effect. This is *not* similar to the results from Galactic A-supergiants, where the mean was  $[\text{Si II}/\text{H}] = -0.2 \pm 0.2$ . Only one line of Si II was observed in only five Galactic stars, but additional Si I abundances were computed in 11 of the cooler Galactic A-supergiants from two lines that yielded  $[\text{Si I}/\text{H}] = -0.1 \pm 0.1$ . It is difficult to understand this trend in the hotter SMC stars, since the analysis of Si II is expected to yield reliable results, although Si III is the dominant ionization stage in these stars meaning that metallicity-dependent NLTE effects might be present.

Derived underabundances of Ca II are consistent with the iron-group underabundances throughout. Ca I is also found for the five coolest stars (primarily from the  $\lambda 4226$  line of multiplet #2), and is in fair agreement with Ca II.

*s-process elements:* Zr II and Ba II have been determined from one or two lines each per star (see Appendix A), and are similar to the iron-group underabundances to within 0.3 dex. This may or may not be a significant difference considering how few lines have been analysed.

Sr II appears more underabundant, with  $[\text{Sr}/\text{Fe}] \leq 1.0$  dex, but NLTE effects are expected for the two Sr II resonance lines used here. Lyubimkov & Boyarchuk (1982) found that Sr abundances measured from the resonance lines are 0.2 to 0.4 dex less than those from a subordinate line in Canopus (F-supergiant) due to NLTE effects. Praderie (1975) found theoretical equivalent widths may be two times smaller in main-sequence A-stars, also due to NLTE effects. The primary Ba indicator in this analysis is also a resonance line. Lyubimkov & Boyarchuk found the same effect for the Ba II resonance lines as for Sr II, however in one star, AV 174, analysed here, the same abundance is determined from a subordinate Ba II line as from the resonance line. Therefore, NLTE effects on the Sr and Ba lines remain uncertain.



## 5. Comparisons with SMC F-K supergiants

The chemical composition of SMC F-K supergiants has been determined by several authors (Russell & Bessell 1989 = RB89, Spite et al. 1989a,b = S89, Luck & Lambert 1992 = LL92, Hill et al. 1997a,b = H97, Luck et al. 1998 = L98). These results are shown in Table 8 as differential abundances, i.e., the abundances listed are the differences between the average for the SMC stars and that of Galactic standard stars as analysed by each individual analysis (see the footnotes to the Table for the standard stars used from each analysis). These differential abundances are a much more accurate and useful way to compare the results from so many different analyses since differential results can minimize the systematic errors per analysis. Differential abundances were first recognized as an improved way to compare abundance data from different Magellanic Cloud objects by Pagel (1992, “like-like” comparisons).

*Iron-group:* The most striking result is that the Fe abundances are essentially identical,  $[\text{Fe II}/\text{H}] \sim -0.6$ . A histogram of Fe determinations from A- through K-type supergiants shows that the scatter within the analyses and between the analyses is very small (Fig. 9). Previously, stars in NGC 330 were thought to be more metal-poor than field stars in the SMC (e.g., Spite et al. 1991, Grebel & Richtler 1992), but recent Fe abundance determinations in F-K supergiants by H97 and Si abundances in B-giants by Korn & Wolf (1998) show no significant differences between the cluster and field stars. Other iron-group elements Sc, Ti, Cr (and Ni in F-K supergiants) also show similar underabundances to Fe ( $\pm 0.2$  dex) in all analyses.

*Carbon:* The differential results (Galactic minus SMC) from F-K supergiants suggest that C has roughly the same underabundance as iron, e.g.  $-0.6$  to  $-0.8$  dex (see Table 8). This may be slightly inconsistent with the nebular and B-star abundances which show slightly larger C underabundances (discussed in Section 6.1), e.g., the nebular C abundance

is about 0.9 dex less than in Orion (and Orion is about 0.3 dex less than solar, c.f., Cunha & Lambert 1994, which conspires to yield SMC  $[C/H]=-1.2$ ).

The upper limit on carbon from AV 174, the coolest star in this analysis, is in better agreement with the lower nebular abundance than the slightly larger F-K supergiant abundance. If mixing of CNO-cycled gas has occurred in AV 174, then this could have lowered C from an initially higher abundance (such as that reported from F-K supergiant analyses), but it seems unlikely that mixing has occurred in this star since N is lowest of all stars examined (see Table 5).

It is unlikely that the F-K supergiant C abundances are in error since several different features of C have been used in the most recent abundance determinations; L98 examined both C<sub>2</sub> molecular features and C I absorption lines, H97 analysed <sup>12</sup>CN, <sup>13</sup>CN, and C<sub>2</sub> molecular features, LL92 measured permitted and (one) forbidden C I line, and S89 and RB89 used C I lines. In the past, the RB89 and S89 supergiant C results were used as an example of the inconsistencies between stellar and nebular abundances in the Clouds, yet those abundances were much higher still (see Table 8). The recent abundances are much more accurate, e.g., RB89 determined C from only one feature in only 2 stars.

*Nitrogen:* Nitrogen abundances in SMC supergiants have a very large range,  $[N/Fe]>1.0$ , but this range is consistent between analyses, i.e., all analyses that include several stars find a wide range in N (see the histogram in Fig. 10). These N abundances have been determined from a variety of features, including N I lines (this paper, LL92), N II lines (R93, Lennon et al. 1996), and molecular CN features (H97, Barbuy et al. 1991). The range itself is not due to uncertainties in the individual analyses, nor due to differences between the analyses (although a small NLTE correction required for early F supergiants can account for the slight offset in the LL92 data due to two stars with  $N>8.0$  in Fig. 10). Thus, the range in N is astrophysically significant and is discussed below in the context of

stellar evolution (Section 6.2).

*Alpha-elements:* The  $\alpha$ -elements typically have the same underabundance as  $[\text{Fe}/\text{H}]$  ( $\pm 0.2$  dex), a result that is consistent between the (differential) results of all of the stellar analyses listed in Table 8, with only a few exceptions. Minor exceptions seen in only one of the analyses can usually be attributed to uncertainties within that analysis, e.g., RB89’s high Ca II abundance was calculated from only one line in one star. Silicon, on the other hand, appears to be slightly overabundant (with respect to iron) in some of the supergiant analyses. Slight silicon overabundances are probably due to uncertainties in the atmospheric analyses, as in the case of the A-supergiants (discussed in Section 5, where the overabundances appear related to temperature). In addition, most other supergiant analyses have  $[\text{Si}/\text{Fe}]=0$ , other  $\alpha$ -elements do not show an overabundance, and the B-stars analysed by Rolleston et al. (1993) have  $[\text{Si}/\text{Fe}]=0$ .

Especially noteworthy is the very good agreement in the O and Fe abundances between the supergiant analyses listed in Table 8, and thus the excellent agreement in the O/Fe ratios. Additionally, the O abundance determined from supergiants is in excellent agreement with that determined from B stars and H II regions (discussed further below). Thus, O/Fe is like the other  $\alpha/\text{Fe}$  ratios in that O and  $\alpha$  elements have the same underabundance as Fe; however it is necessary to report  $[\text{O}/\text{Fe}]=-0.2$  because the Sun is slightly O rich relative to the solar neighborhood (discussed further below).

*s-process elements:* Good agreement is found between the three s-process elements examined here in the A-type supergiants (Sr, Zr, and Ba) and F-K supergiant results. These three elements share the underabundances of the iron-group elements, and are often slightly lower. Sr by RB89 and herein should not be weighed too heavily since RB89 measured only one (strong, 394 mÅ) line in only one star, and the A-supergiant Sr suffers from neglected NLTE line formation effects.

## 6. Stellar Evolution

Elemental abundances can be used to examine the evolutionary status of a star since hydrogen-burning occurring in interior layers may be mixed with pristine gas at the surface of a star during its evolution. Since massive stars burn hydrogen primarily via the CNO-cycle, then the ratios of these catalysts change in a predictable way. Although many evolution scenarios exist, few are well constrained by the observations for massive stars, particularly for low metallicities (c.f., Langer & Maeder 1995, Maeder & Conti 1994, Stothers & Chin 1992). For example, the conditions as to when massive stars burn helium as blue or red supergiants remain uncertain, and the evidence of CN-cycled gas at the surfaces of main-sequence B-stars (which are expected to have pristine, unmixed, abundances) is puzzling.

Most stellar evolution scenarios at low metallicities predict that massive stars burn helium in their cores as blue supergiants. As an example, Schaller et al. (1992) predict that stars with  $M < 20 M_{\odot}$  burn helium while evolving along a blue loop, while stars  $\geq 20 M_{\odot}$  burn helium while evolving directly towards the red giant branch. In this scenario, the most massive blue supergiants would have unaltered CNO abundances, while the less massive blue supergiants would have first dredge up abundances (where the change in the  $12+\log(X/H)$  abundances are predicted as C: N: O  $\sim -0.2: +0.5: -0.05$ ). This is a testable prediction.

The assumptions required for massive star evolution models are poorly constrained though, such that blue loops may not exist at all, or perhaps all stars burn helium as blue supergiants at low metallicities (as either post- or pre- red supergiants). Langer & Maeder (1995, their Fig. 1) show an additional complication; in their investigation of semiconvection at  $z=0.002$ , they predicted three different evolutionary scenarios for three different masses, 15, 20, and  $25 M_{\odot}$ , in otherwise identical models. Helium burning occurs during a blue-loop

at  $15 M_{\odot}$ , during the red supergiant phase at  $20 M_{\odot}$ , and as a post-main-sequence blue supergiant at  $25 M_{\odot}$ . Clearly, reliable abundances of CNO for blue supergiants in the Magellanic Clouds will help to constrain these models.

Additionally, the effects of rapid rotation on massive stars have been investigated theoretically for Galactic stars (Maeder 1987, Dennisenkov 1994, Fliegner et al. 1996, Meynet 1997, Maeder & Zahn 1997, Talon et al. 1997, Langer & Heger 1998), as well as LMC stars (Langer 1991). With respect to abundances, star-to-star variations of light elements in some Galactic OB-stars and blue supergiants require a more discrete parameter like rotation rate. A few main-sequence B-stars were reported to have enhanced N (Gies & Lambert 1992), while several B and A-supergiants are also slightly N enhanced (Venn 1995a, Lennon 1994). In addition, boron is expected to be destroyed by partial mixing on the main-sequence so that a B-N trend should exist, although at present very few boron abundances are available for an examination (c.f., Venn et al. 1996, Cunha et al. 1997). As rotation rate is a metallicity-*independent* parameter, then partial mixing may also affect the Magellanic Cloud stars.

### 6.1. Initial CNO Abundances

To interpret the CNO abundances in Magellanic Cloud stars in the context of stellar evolution, it is necessary that we know initial as well as current abundances to look for signs of mixing. The best way to estimate the initial abundances of young stars is by examining CNO from nebular abundances and from main-sequence B-stars. Since CNO each have different nucleosynthetic sites from each other and from Fe-group elements, it is *not* sufficient to assume that they scale with the overall metal underabundance of the SMC (as has often been assumed in previous analyses).

Nebular abundances in the Magellanic Clouds have been determined by several investigators (c.f., Dufour 1984, 1990; Pagel 1992). More recent SMC nebular analyses done with modern detectors have been reported by Russell & Dopita (1990), Garnett et al. (1995), and Kurt et al. (1998). These abundances are discussed further below. On the other hand, only a few calculations of abundances in unevolved B-stars in the SMC exist (Rolleston et al. 1993 = R93), but these should reflect those of the interstellar medium.

For carbon, absolute abundances from B-dwarfs in the SMC are very uncertain due to NLTE effects of the C II feature analysed. For example, R93 report an *absolute* abundance for carbon of  $12+\log(\text{C}/\text{H})=6.9$ , significantly lower than the nebular abundance; but, taking the mean of the Galactic B-stars and subtracting the *differential* abundance for the SMC B-stars yields,  $12+\log(\text{C}/\text{H})=8.3 - 0.9 = 7.4$ , in perfect agreement with the nebular abundances (see Table 10). R93 also comment that this is the correct way to interpret their C abundance because NLTE is expected to strongly affect their C II  $\lambda 4267$  feature. The fact that the SMC B-star C abundance agrees well with the SMC nebular result is significant since it implies that depletions of C onto dust grains in the ISM are small! This result has also been found for nebular and B star C abundances in Orion.

Mathis (1996) reviews and discusses the observations of CNO in the interstellar medium in the Galaxy. Very little N is expected to be in dust, however only 2/3 of the O atoms and half of the C atoms are thought to be in the gas-phase (also supported by more recent observations by Meyer et al. 1998 and Sofia et al. 1997). Thus, the nebular abundance of N should be the same as young B-stars, but nebular C and O should be slightly less than the B star abundances, by roughly 0.15 dex and 0.3 dex, respectively. Such large differences between nebular and B star abundances are not seen though; for example, the nebular and B star abundances in Orion are in excellent agreement (see Table 9; also discussed by Mathis 1996). Recently, Esteban et al. (1998) adopted slightly smaller dust correction

factors for C and O,  $\leq 0.1$  dex for their Orion gas abundances. These smaller corrections are well within the 1 to  $2\sigma$  uncertainties in the stellar abundances.

Assuming that global metallicity does not change the element depletion fractions of the gas-phase ISM too significantly, then the nebular and B star CNO abundances should be in good agreement in the SMC as well. Thus, the agreement between the nebular and B stars C abundance strongly suggests that  $12+\log(\text{C}/\text{H})=7.4$  is the correct present-day C abundance, as opposed to the higher C abundance reported from the F-K supergiants. Ironically, the difference between the F-K supergiants and the nebular/B-stars C abundance is about +0.3 dex, which is the predicted interstellar dust depletion factor for the ISM. For this paper, the present-day C abundance is not critical since upper limits only have been determined for C in A-type supergiants, however the present-day N abundance is critical.

The SMC nebular nitrogen abundances are very low,  $12+\log(\text{N}/\text{H})=6.6$ ; this has been determined by Dufour (1984) and RB89 assuming  $\text{N}^+/\text{O}^+ = \text{N}/\text{O}$ , which Garnett (1990) showed is sufficient for an accurate N abundance in low metallicity galaxies from photoionization model tests. As further confirmation, recent  $\text{N}^{++}/\text{O}^{++}$  measurements (Garnett et al. 1995, Kurt et al. 1998) of one high excitation nebula, SMC N88A, has resulted in a similar low N abundance, see Table 10. In addition, grain depletion of N is expected to be negligible (see above), and since  $\text{N}^+/\text{O}^+$  and  $\text{N}^{++}/\text{O}^{++}$  yield such similar results, then this implies that the ionization corrections are well established. In the B-stars, only an upper limit on the N abundance is available because no N II lines were observed (a marginal detection of a single N III line in one star yields consistent results but is uncertain due to a blend with an O II line). Thus, the nebular N abundance is adopted in this paper as the initial abundance for the supergiants.

The abundance for oxygen determined from the SMC B-stars is in excellent agreement with that from the SMC nebulae (both absolute and differential O abundances are in

agreement),  $12+\log(\text{O}/\text{H})=8.1$ , as seen in Table 10. This value is also found from analyses of evolved B-stars (Reitermann et al. 1990, Jüttner et al. 1992, Rolleston et al. 1993, Lennon et al. 1996, Korn & Wolf 1998) and is consistent with the differential results for F-K supergiants (see Table 8).

## 6.2. Implications for Massive Star Evolution

For Galactic stars, examination of CNO in supergiants is not too difficult since detailed abundance analyses of CNO have been done for over 70 B-stars in the solar neighborhood and nebular abundances are available for Orion and other H II regions throughout the Galactic disk (see Table 9 for references and results). From these analyses, evidence for slight mixing of CN-cycled gas has been found in some main-sequence B-stars and B-giants (Gies & Lambert 1992, Lennon 1994), as well as in the A-type supergiants analysed by Venn (1995a,b). This can be seen in a histogram of the N abundances (Fig. 10), by the slight high-end tail in the Galactic B-stars, and the offset from the initial N abundance in the Galactic A-type supergiants. In the SMC, only 3 main-sequence B-stars have been examined in detail, but there are more data from nebular abundances (see Table 10). The initial CNO abundances adopted here are the best available, however they remain a major source of uncertainty, especially for C which differs by 0.3 dex from F-K supergiant analyses (see discussion above in Section 6.1). An effort for more abundance analyses of main-sequence B-stars in the Magellanic Clouds should be undertaken when larger telescopes and/or higher efficiency spectrographs are available at the southern observatories.

To examine the evolutionary status of the SMC A-supergiants, we need to examine the N abundances for signs of mixing of CN-cycled gas. Normally, one likes to examine the N/C ratio since both C and N are affected by mixing (and the sum of the catalysts, C+N+O, remains constant), but only upper limits were obtained for C, and nevertheless N is the



element most affected. The majority of A-supergiants in the SMC show N enrichments over the nebular/B-star abundance. The amount of the enrichment varies from  $\leq 0.2$  dex to  $\geq 1.2$  dex! This range is large, and suggests that enrichments can vary drastically from star-to-star. A similar phenomenon is seen in the SMC B-giants, since Lennon et al. (1996) found that two B-giants in NGC 330 appear to be very enriched in N, yet two other B-giants in the same cluster analysed by Jüttner et al. (1992) report the opposite.

The range, from close to the initial N value to well beyond the first dredge-up value, cannot be due to atmospheric uncertainties, e.g., Fig. 9 shows the range in N is much larger than for O or Fe. In addition, the median value is greater than the predicted first dredge-up abundance (of  $\sim +0.6$  dex). Perhaps all of these stars are post-red supergiants, however this ignores the fact that some stars appear to have undergone little or no mixing. If most stars have undergone the first dredge-up, and only a few are post-main-sequence stars, then this could account for the lower N values (standard models predict only 1 in 50–100 stars in this mass range would be post-main sequence stars, yet some models, e.g., Langer & Maeder, 1995, predict closer to even numbers); but the highest N abundances still remain unexplained.

The fact that partial mixing is indicated in the Galactic stars affects the interpretation of the SMC abundances – perhaps most SMC stars undergo partial mixing, in addition to the first dredge-up. If so, this could account for the highest N abundances (first dredge-up and extreme rotational mixing), as well as the lowest results (slight rotational mixing only). Of course, this implies a mixed population of A-type supergiants, including both post-RGB and post-MS stars, but this is already predicted by many evolution scenarios (e.g., Schaller et al. 1992, Bertelli et al. 1994, Langer & Maeder 1995).

Now the question becomes “could rotational mixing account for the N abundances entirely?” At present, only the most rapid rotators are expected to undergo significant

main-sequence mixing that would enrich N as efficiently as the first dredge-up. Therefore, if rotational mixing is entirely responsible, then main-sequence mixing must be more efficient in metal-poor stars. This means the stars must all rotate rapidly. Although data on rotation rates in SMC main-sequence B-stars is scant, this seems rather unlikely.

Although carbon abundances could not be determined here as a further test of this interpretation, there is one other element that may be an indicator of mixing – sodium. In this paper, A-supergiant  $[\text{Na}/\text{Fe}]$  is near solar, which is similar to the recent results by L98 for F-K supergiants. L98 interpret their *lack* of an overabundance as evidence *against* mixing processes, assuming that enrichments of Na occur due to mixing of Ne-Na cycled gas. This interpretation is complicated though, in part because several different explanations have been proposed to explain Na enrichments in Galactic stars (see Lambert 1992), but more importantly because we do not know the initial Na abundance in the SMC.

One way to use Na though is to look for a Na-N or Na-O trend. If Ne-Na cycled gas has mixed to the surface, then CN-cycle/ON-cycled gas would accompany it since those cycles run at cooler/similar temperatures. Any mixing of primary Na must also enrich secondary N (and deplete C and O). Plots of Na versus N and O are shown in Fig. 11. It might be possible to see some hint of a trend in the data (e.g., Na increasing with N, but decreasing with O), but nothing significant because of the large scatter in the data. Theoretical first dredge-up values (for classical non-rotating stellar evolution models by Heger 1998) are shown in Fig. 11 by arrows (adopting initial abundances for N and O from Table 10, and assuming  $[\text{Na}/\text{Fe}]=0$ ).

## 7. Chemical Evolution of the SMC

Several chemical evolution models exist for the SMC, in which various assumptions are invoked (e.g., inflow of unprocessed gas, Russell & Doptia 1992, steeper IMF, Tsujimoto et al. 1995) to reproduce the low  $\alpha$  element abundances determined from stars, planetary nebulae, supernovae, and H II regions, relative to the solar neighborhood. The ratio of, for example, O/Fe is an important constraint since these elements have different nucleosynthetic sites; oxygen is primarily produced in Type II supernovae events, while iron comes from all supernovae, including SN Ia during quiescent intervals (Gilmore & Wyse 1991). More recently, Pagel & Tautvaišienė (1998) have suggested that large variations on the Galactic chemical evolution models are not necessary to reproduce the abundances, partially because the  $\alpha$ -element abundances are not unusually low when considered in “like-like” analyses with their Galactic counterparts. Pagel & Tautvaišienė assume the same yields and time delays as for their solar neighborhood chemical evolution models to produce analytical chemical evolution models for the Magellanic Clouds.

It is certainly true that oxygen is not unusually low when examined relative to Orion or the solar neighborhood, and not to the Sun. When oxygen is examined this way, then the SMC underabundance of O is similar to that of Fe (discussed in Section 5). For example,  $12+\log(\text{O}/\text{H})=8.9$  in the Sun, but only  $12+\log(\text{O}/\text{H})=8.6$  from B-stars in the solar neighborhood, B-stars in Orion, and nebular Orion abundances (see Table 9).  $12+\log(\text{O}/\text{H})=8.6$  is also the average determined from analyses of young F-K supergiants (e.g., Luck & Lambert 1985, Barbuy et al. 1996, L98), A-type supergiants (Venn 1995a, with NLTE corrections cited in Section 4), and some B-type supergiants (e.g., Lennon et al. 1991, Gies & Lambert 1992) in the Galaxy. Oxygen abundances in the SMC are  $-0.5$  dex from this value, as determined by the B-stars and nebulae (see Table 10), which is supported by the abundances found from SMC supergiants (see Table 8). Thus,  $[\text{O}/\text{Fe}]=-0.2$  (recalling

that the square bracket notation denotes an abundance relative to the Sun), but more accurately the differential abundances are  $\log(\text{O}/\text{Fe})_{\text{smc}} - \log(\text{O}/\text{Fe})_{\text{gal}} = +0.1$ .

A similar result is found for the other  $\alpha$ -elements. In this analysis, the abundance of Mg is particularly well determined – Mg II is almost insensitive to uncertainties in the stellar parameters (see Tables 4 & 6), yielding a very reliable abundance.  $[\text{Mg}/\text{Fe}] = 0$  in the SMC A-supergiants (see Table 7). Similar underabundances have been found from other analyses of SMC F-K supergiants, and B-stars (see Table 8), but from fewer lines that are more sensitive to atmospheric uncertainties in both cases.

Other  $\alpha$ -elements determined here include Si, Ca and Ti (which acts like an  $\alpha$ -element in Galactic stars; c.f., Edvardsson et al. 1993, and the discussion by Wheeler et al. 1989). Si II abundances in the A-type supergiants appear to be uncertain in some supergiant analyses (discussed in Section 4). The Ca abundances from Galactic A-supergiants are not consistent, with  $[\text{Ca I}/\text{H}] = +0.3$  and  $[\text{Ca II}/\text{H}] = -0.3$ . Examining only the Ca II abundances, which should be better determined in these stars since Ca II dominates the ionization balance over Ca I (where NLTE effects may be strong), then the like-like depletion of Ca in the SMC is  $\sim 0.7$  dex, in excellent agreement with O and Mg. This abundance is also in good agreement with the Ca I abundances determined in F-K supergiants (see Table 8). Ti II is well determined in both Galactic and SMC A-supergiants. Even though the abundances are rather sensitive to the atmospheric parameters, there are many absorption lines available over a range of wavelengths, line strengths, and formation depths.  $[\text{Ti}/\text{H}] = -0.6$  dex in the SMC A-supergiants, in agreement with the other  $\alpha$ -elements. The reliable Ti II abundances determined in A-supergiants are also an excellent complement to, and in good agreement with, the reliable Ti I abundances determined in the F-K supergiants.

For comparison to the Galaxy, we have the incredible efforts by Edvardsson et al. (1993) who have determined abundances in 189 field F-G disk dwarf stars. Metal abundances range

from  $-0.8 \leq [\text{Fe}/\text{H}] \leq +0.2$ , with an estimated accuracy of  $\pm 0.05$  dex. Their analyses find that O, Mg, and other  $\alpha$ -elements do not track the Fe depletions, but instead are slightly less depleted than Fe at low metallicities. At the SMC metallicity of  $[\text{Fe}/\text{H}] \sim -0.6$ , then  $[\text{O}, \text{Mg}/\text{Fe}] \sim +0.2$  to  $+0.3$ , and  $[\text{Si}, \text{Ca}, \text{Ti}/\text{Fe}] \sim +0.15$ . In addition, Tomkin et al. (1995) found  $[\text{C}/\text{Fe}] \sim +0.3$ . The Galactic overabundances of  $\alpha$ -elements at low Fe are not seen in the SMC. The young stars and nebulae in the SMC show present-day, young Galactic abundance ratios to within their  $1\text{-}\sigma$  uncertainties. These abundance ratios are reproduced by the latest chemical evolution models of Pagel & Tautvaišienė (1998).

Finally, the light s-process elements determined here can also be used to examine some details of the SMC’s chemical evolution. In particular, Pagel & Tautvaišienė (1998) consider different star formation rate (SFR) histories – one which has been constant over time (“smooth” model), and another with punctuated episodes of star formation (“bursting” model). The change in the SFR history can affect the age-metallicity diagram for the SMC as well as the certain present-day s-process elemental abundances. In this paper,  $[\text{Zr} \& \text{Ba}/\text{Fe}] = -0.2$  to  $-0.4$ , in agreement with most F-K supergiant analyses (see Table 8).  $[\text{Sr}/\text{Fe}] = -0.6$  is also in good agreement with results by RB89, yet suffers from significant analysis uncertainties (discussed in Section 4). These less-than-solar ratios favor Pagel & Tautvaišienė’s bursting model, i.e., their bursting model predicts  $[\text{Y}, \text{Zr} \& \text{Ba}/\text{Fe}] \sim -0.2$  at present. In their smooth SFR models, solar-like ratios are predicted. It is not possible to distinguish between their bursting and smooth models using any other element ratios (e.g.,  $\alpha$ - or Fe-group elements). Pagel & Tautvaišienė’s models also make predictions for other (heavier) s&r-process elements not discussed here (i.e., not observed in A-supergiant spectra). Abundance predictions for those other elements (e.g., Ce, Nd, Eu) are in poor agreement with the observed abundances from F-K supergiant analyses, although the uncertainties in those derived abundances are also quite significant (e.g., those abundances are often based on only a few spectral lines with large line-to-line scatter). Recently,

DaCosta & Hatzidimitriou (1998) have used abundance determinations based on the Ca II triplet in red giants in SMC clusters to suggest that the simpler, smooth model reproduces the age-metallicity trend in the SMC. However, Mighell et al. (1998) have analysed HST color-magnitude diagrams of the same clusters (mostly) and determined ages, metallicities, and reddenings that may favor the bursting model – in agreement with the Zr and Ba abundances presented here.

## 8. Conclusions

Analysis of 10 A-type supergiants in the SMC has shown that atmospheric parameters and elemental abundances can be well determined in a tailored analysis (including ATLAS9 LTE model atmospheres, weak lines from dominant ionization stages, and NLTE line formation only when necessary). The atmospheric parameters show that previously assigned spectral types are often incorrect, which had resulted in some stars being erroneously classified as helium-rich anomalous stars.

New elemental abundances of N, O, Na, Mg, Si, Ca, Sc, Ti, Cr, Fe, Sr, Zr, and Ba have been determined.  $[\text{Fe}/\text{H}] = -0.7 \pm 0.07$ , but with respect to Galactic A-type supergiants this is reduced to  $-0.6$  dex. This result is in excellent agreement with those from F-K supergiants, and with other iron-group elements (Ti, Cr).  $\alpha$ -elements have the same underabundances as iron-group elements, including Mg, Si, and Ca.  $[\text{O}/\text{Fe}] = -0.2$ , but considering that the Sun is overabundant in oxygen by 0.3 dex, then actually O has the same underabundance as iron (within 0.1 dex). This is in agreement with the *differential* B star abundance, the *differential* F-K supergiant results, and the the nebular analyses. Certain s-process elements are more underabundant than iron,  $[\text{Sr}, \text{Zr}, \text{Ba}/\text{Fe}] \leq 0.3$  dex, in good agreement with results from F-K supergiants.

The N abundances in the SMC A-supergiants strongly suggest that these stars have undergone the first dredge-up, as is currently predicted by most SMC stellar evolution theories. The large range in these abundances suggests that there are additional star-to-star variations though, most likely related to effects of rotational mixing on the main-sequence (not currently included in most stellar evolution theories, but possibly having wide reaching implications on massive star ages and masses). In addition, a few stars appear to have very low N suggesting that they may be evolving from the main-sequence only now and have not yet undergone the first dredge-up.

O, Mg, and other  $\alpha$ -elements show similar depletions as Fe relative to Galactic standards. This is different from metal-poor stars in the solar neighborhood. The SMC galaxy evolution model by Pagel & Tautvaišėnė (1998) reproduce these abundances. In addition, higher depletions of certain s-process elements (Zr, Ba) favor their model with a bursting star formation rate.

Many thanks to Rolf-Peter Kudritzki for making this project possible by giving me the opportunity to work with him at the Universität-Sternwarte-München & MPA-Garching. I am indebted to Danny Lennon for many valuable conversations about hot stars and the Magellanic Clouds, to Evan Skillman and Don Garnett for several discussions on nebular abundances, to Michael Lemke for advice and help on NLTE analyses, and to Norbert Langer for guidance in stellar evolution. This project has been supported in part by a Max Planck Institute post-doctoral fellowship and a Clare Boothe Luce Professorship grant. Travel support by the European Southern Observatory is gratefully acknowledged, as well as superior observing advice and assistance.

## REFERENCES

- Anders E., Grevesse N. 1989, *Geochim. Cosmochim. Acta*, 53, 197
- Ardeberg, Maurice 1977, *A&AS*, 30, 261
- Azzopardi M., Vigneau J. 1982, *A&AS*, 50, 291
- Baldwin J.A., Ferland G.J., Martin P.G., Corbin M.R., Cota S.A., Peterson B.M., Slettebak A., 1991, *ApJ*, 374, 580
- Barbuy B., De Medeiros J.R., Maeder A., 1996, *A&A*, 305, 911
- Barbuy B., Spite M., Spite F., Milone A., 1991, *A&A*, 247, 15
- Baschek B., Scholz M., Sedlmayr E., 1977, *A&A*, 55, 375
- Bertelli G., Bressan A., Chiosi C., Fagotto F., Nasi E., 1994, *A&AS*, 106, 275
- Biémont E., Grevesse N., Hannaford P., Lowe R.M., 1981, *ApJ*, 248, 867
- Boyarchuk A.A., Lyubimkov L.S., Sakhbullin N.A., 1985, *Astrophysics*, 22, 203
- Cunha K., Lambert D.L. 1994, *ApJ*, 426, 170
- Cunha K., Lambert D.L., Lemke M., Gies D.R., Roberts L.C., 1997, *ApJ*, 478, 211
- Da Costa G.S., Hatzidimitriou D., 1998, *AJ*, 115, 1934
- Denissenkov P.A., 1994, *A&A*, 287, 113
- Dopita M., Vassiliadis E., Wood P.R., Meatheringham S.J., Harrington J.P., Bohlin R.C., Ford H.C., Stecher T.P., Maran S.P., 1997, *ApJ*, 474, 188
- Drake J.J., Lambert D.L., 1994, *ApJ*, 435, 797



- Dufour R.J., 1984 in *Structure and Evolution of the Magellanic Clouds*, IAU Symp. 108, eds. S. van den Bergh and K.S. de Boer (Reidel:Dordrecht), p. 353
- Dufour R.J., 1990 in *Evolution in Astrophysics: IUE Astronomy in the Era of New Space Missions*, eds. E.J. Rolfe, ESA-SP-310, p.117
- Dufton P.L., Fitzsimmons A., Howarth I.D. 1990 ApJ 362, L59
- Edvardsson B., Andersen J., Gustafsson B., Lambert D.L., Nissen P.E., Tomkin J., 1993, A&A, 275, 101
- Esteban C., Peimbert M., Torres-Peimbert S., Escalante V., 1998, MNRAS, 295, 401
- Fitzpatrick E.L., Garmany C.D. 1990, ApJ, 363, 119
- Fitzpatrick E.L., 1991, PASP, 103, 1123
- Fliegner J., Langer N., Venn K.A., 1996, A&A, 308, L13
- Fuhr J.R., Martin G.A., Wiese W.L., 1988, J. Phys. Chem. Ref. Data, 17, Suppl. No. 4
- Fuhr J.R., Martin G.A., Wiese W.L., Younger S.M., 1981, J. Phys. Chem. Ref. Data, 10, 305
- Garnett D.R., 1990, ApJ, 363, 142
- Garnett D.R., Skillman E.D., Dufour R.J., Peimbert M., Torres-Peimbert S., Terlevich R., Terlevich E., Shields G.A. 1995 ApJ, 443, 64 (G95)
- Gilmore G., Wyse R.F.G., 1991, ApJ, 367, L55
- Grebel E., Richtler T., 1992, A&A, 253, 359
- Gies D.R., Lambert D.L. 1992, ApJ, 387, 673
- Gigas D. 1986, A&A, 165, 170

- Gigas D. 1988, A&A, 192, 264
- Grevesse N., Noels A., 1993, in *Origin and Evolution of the Elements* eds. N. Prantzos, E. Vangioni-Flam, M. Cassé (CUP; Cambridge), p. 15.
- Heger A., 1998, Ph.D. thesis, University of Munich and the Max Planck Institute for Astrophysics.
- Hibbert A., Biémont E., Godefroid M., Vaeck N., 1991, J. Phys. B, 24, 3943
- Hill V., Barbuy B., Spite M., 1997a, A&A, 323, 461 (H97a)
- Hill V., 1997b, A&A, 324, 435 (H97b)
- Hill V., 1998, in *New Views on the Magellanic Clouds*, eds Y.H. Chu, N. Suntzeff, in prep.
- Humphreys R.M. 1983, ApJ, 265, 176
- Humphreys R.M., Kudritzki R.P., Groth H. 1991, A&A, 245, 593
- Jüttner A., Stahl O., Wolf B., Baschek B. 1992 in *New Aspects of Magellanic Cloud Research*, eds B. Baschek, G.Klare, J.Lequeux (Springer-Verlag: Berlin), 337
- Kaufer A., Stahl O., Wolf B., Gaeng T., Gummersbach C.A., Jankovics I., Kovacs J., Mandel H., Peitz J., Rivinius T., Szeifert T., 1996, A&A, 314, 599
- Kilian J. 1992, A&A, 262, 171
- Korn A., Wolf B. 1998 in *New Views on the Magellanic Clouds*, eds Y.H. Chu, N. Suntzeff, in prep.
- Kurt C.M., Dufour R.J., Garnett D.R., Skillman E.D., Mathis J.S., Peimbert M., Torres-Peimbert S., Ruiz M.T., 1998, preprint

- Kurucz R.L. 1969, in *Proc. Third Harvard-Smithsonian Stellar Atmospheres Conf.*, ed. O. Gingerich, (MIT Press: Cambridge), p. 375.
- Kurucz R.L. 1979, *ApJS*, 40, 1
- Kurucz R.L., 1988, *Transactions of the IAU*, Vol. XXB, ed. D. McNally (Kluwer: Dordrecht), 168
- Kurucz R.L., 1990, *Trans IAV B*, 20, 168 (magnetic tape)
- Kurucz R.L., 1991, private communication
- Lambert D.L., 1992, in *Instabilities in Evolved Super and Hypergiants*, eds. C de Jager & H. Nieuwenhuijzen (Amsterdam: North-Holland), p. 156
- Langer N., 1991, *A&A*, 243, 155
- Langer N., Maeder A., 1995, *A&A*, 295, 685
- Langer N., Heger A., 1998 in *New Views on the Magellanic Clouds*, eds Y.H. Chu, N. Suntzeff, in prep.
- Lemke M., Venn K.A., 1995, *A&A*, 309 558
- Lennon D.J., Becker S.T., Butler K., Eber F., Groth H., Kunze D., Kudritzki R.P., 1991, *A&A*, 252, 498
- Lennon D.J. 1994, *Space Sci. Rev.*, 66, 127
- Lennon D.J., Dufton P.L. Mazzali P.A., Pasian F. Marconi G., 1996, *A&A*, 314, 243
- Lennon D.J. 1997, *A&A*, 317, 871
- Luck R.E., Lambert D.L. 1985 *ApJ*, 298, 782

- Luck R.E., Lambert D.L. 1992 ApJS, 79, 303 (LL92)
- Luck R.E., Moffett T.J., Barnes T.G., Gieren W.P., 1998, AJ, 115, 605 (L98)
- Lyubimkov L.S., Boyarchuk A.A., 1982, Astrofizika, 18, 596
- Maeder A., 1987, A&A, 178, 159
- Maeder A., Conti P.S., 1994, ARA&A, 32, 227
- Maeder A., Meynet G. 1989, A&A, 210, 155
- Maeder A., Zahn J.P., 1998, A&A, 334, 1000
- Martin G.A., Fuhr J.R., Wiese W.L., 1988, J. Phys. Chem. Ref. Data, 17, Suppl. No. 3
- Mathis J.S., 1996, ApJ, 472, 643
- McCarthy J.K., Lennon D.J., Venn K.A., Kudritzki R.P., Puls J., Najarro F., 1995, ApJ, 455, L135
- Meyer D.M., Jura M., Cardelli J.A., 1998, ApJ, 493, 222
- Meynet G. 1997, in *Boulder-Munich II: Properties of Hot, Luminous Stars*, ed. Ian Howarth (ASP: San Francisco), p.96
- Mighell K.J., Sarajedini A., French R.S., 1998, AJ, 116, 2395
- O'Brian, T.R., Wickliffe M.E., Lawler J.E., Whaling W., Brault J.W., 1991, J. Opt. Soc. Am. B, 8, 1185
- Osterbrock D.E., Tran H.D., Veilleux S., 1992, ApJ, 389, 305
- Pagel B.E.J., 1992, in *New Aspects of Magellanic Cloud Research*, ed. G. Klare (Springer-Verlag:Heidelberg), p.330

- Pagel B.E.J., Tautvaišienė G., 1995, MNRAS, 276, 505.
- Pagel B.E.J., Tautvaišienė G., 1998, MNRAS, 299, 535.
- Peimbert M., 1993, Revista Mexicana de Astronomia y Astrofisica, 27, 9
- Praderie F., 1975, in *Physics of Ap-Stars* IAU Coll. No. 32, eds. W.W. Weiss, H. Jenkner, and H.J. Wood (Universitaetssternwarte Wien:Vienna), p.201
- Przybilla N., 1997, Diplomarbeit, Universität München
- Reitermann A., Baschek B., Stahl O., Wolf B. 1990 A&A 234, 109
- Richtler T., Spite M., Spite F., 1991, in *The Magellanic Clouds*, eds R. Haynes and D. Milne, 374.
- Rolleston W.R.J., Dufton P.L., Fitzsimmons A., Howarth I.D., Irwin M.J. 1993, A&A, 277, 10 (R93)
- Rubin R.H., Simpson J.P., Haas M.R., Erickson E.F., 1991, ApJ, 374, 564
- Russell S.C., Bessell M.S. 1989, ApJS, 70, 865 (RB89)
- Russell S.C., Dopita M.A. 1990 ApJS, 74, 93
- Russell S.C., Dopita M.A. 1992 ApJ, 384, 508
- Sanduleak N. 1969, Contr. Cerro Tololo Int. Am. Obs. 89
- Schaller G., Schaerer D., Meynet G., Maeder A. 1992, A&AS, 96, 269
- Sigut T.A.A., Landstreet J.D., 1990, MNRAS, 247, 611
- Sofia U.J., Cardelli J.A., Guerin K.P., Meyer D.M., ApJ, 482, L105
- Spite F., Richtler T., Spite M. 1991, A&A, 252, 557

- Spite M., Spite F., Barbuay B., 1989a, A&A, 222, 35 (S89a)
- Spite F., Spite M., Francois P. 1989b, A&A, 210, 25 (S89b)
- Spite M., Spite F., 1990, A&A, 234, 67
- Stothers R.B., Chin C., 1992, ApJ, 390, L33
- Stürenburg S., Holweger H., 1990, A&A, 237, 125
- Takeda Y., 1992, PASJ, 44, 309
- Takeda Y., 1994, PASJ, 46, 181
- Tomkin J., Woolf V.M., Lambert D.L., Lemke M., 1995, ApJ, 453, 660
- Tsujimoto T., Nomoto K., Yoshii Y., Hashimoto M., Yanagida S., Thielemann F.K., 1995,  
MNRAS, 277, 945
- Venn K.A., 1993, ApJ, 414, 316
- Venn K.A., 1995a, ApJ, 449, 839
- Venn K.A., 1995b, ApJS, 99, 659
- Venn K.A., Lambert D.L., Lemke M., 1996, A&A, 307, 849
- Venn K.A., McCarthy J.K., Lennon D.J., Kudritzki R.P., 1998, in *Abundance Profiles:  
Diagnostic Tools for Galaxy History*, eds. D. Friedli, M. Edmunds, C. Robert, L.  
Drissen (ASP: San Francisco) p.54
- Walter D.K., Dufour R.J., Hester J.J., 1992, ApJ, 397, 196
- Wiese W.L., Martin G.A., 1980, NSRDS-NBS, 68
- Wiese W.L., Smith M.W., Miles B.M., 1969 NSRDS-NBS, 22

Wheeler J.C., Sneden C., Truran J., 1989, *ARA&A*, 27, 279

Zhu Q., Bridges J.M., Hahn T., Wiese W.L., 1989, *Phys. Rev. A*, 40, 3721

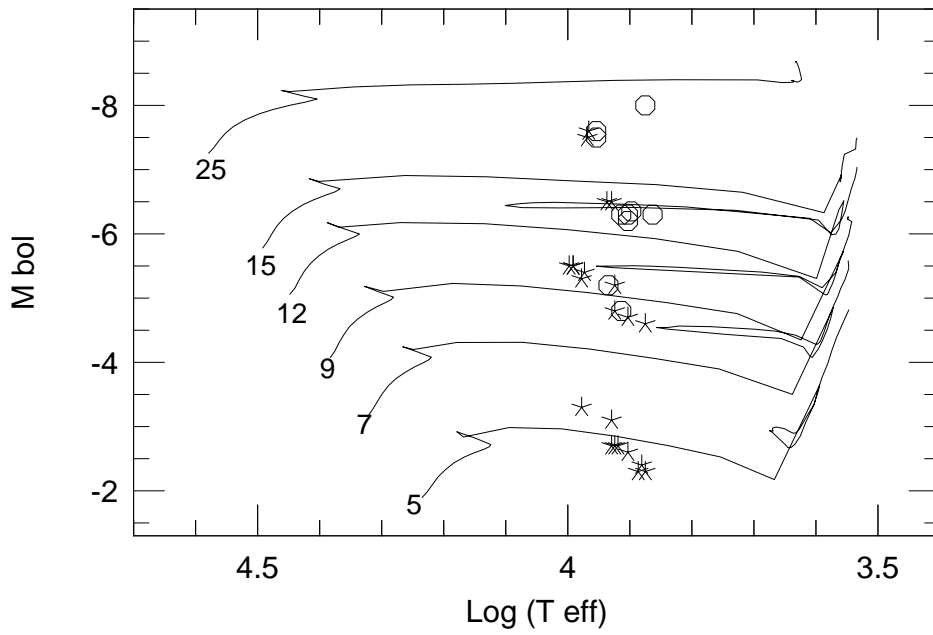


Fig. 1.— HR-diagram of SMC (*empty circles*) and Galactic (*stars*) A-supergiants analysed in this paper and by Venn (1995a,b). Standard stellar evolution tracks from Schaller et al. (1992) are shown.



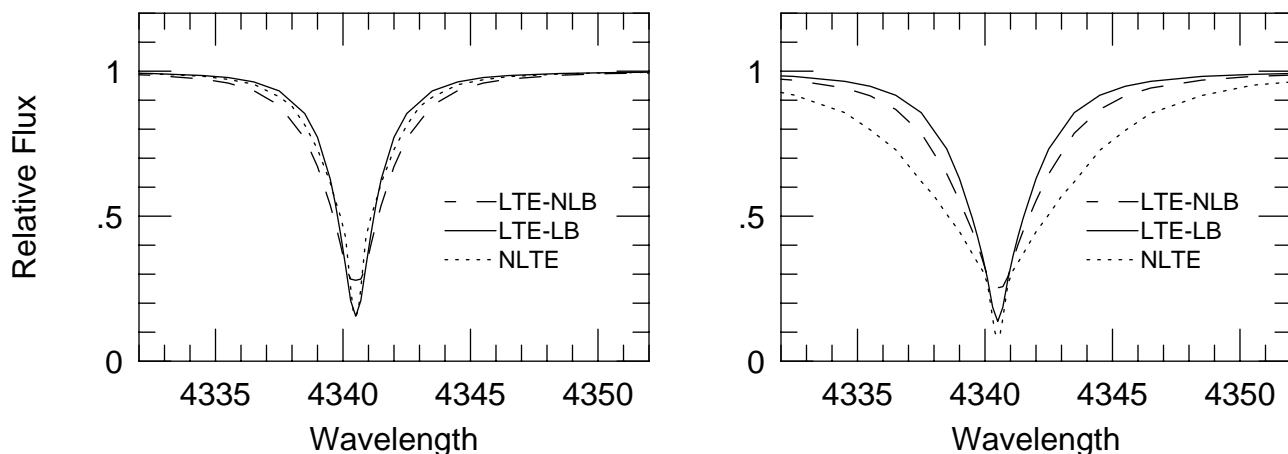


Fig. 2.— Profiles of  $H\gamma$  from three different sets of model atmospheres with  $T_{\text{eff}}=8800$  K and  $\log g=1.1$  (left panel) and  $\log g=1.3$  (right panel). Solid lines from Kurucz’s ATLAS9 including detailed ODFs. Dashed lines from Kurucz’s ATLAS8 with only H and He bound-free edges (no ODFs). Dotted lines are from Kunze’s NLTE models with H and He edges only (Kudritzki, private communications). All models yield very similar  $H\gamma$  line profiles at low gravity, but not at high gravity.

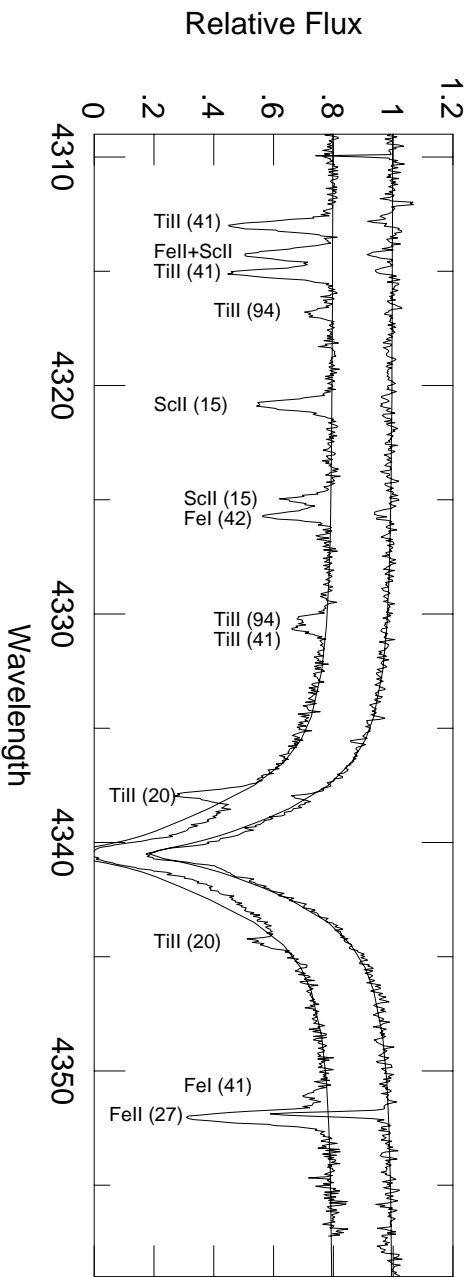


Fig. 3.— Sample spectra of AV 298 (upper) and AV 442 (lower) in the H $\gamma$  region. Theoretical profiles from ATLAS9 using the atmospheric parameters listed in Table 1.

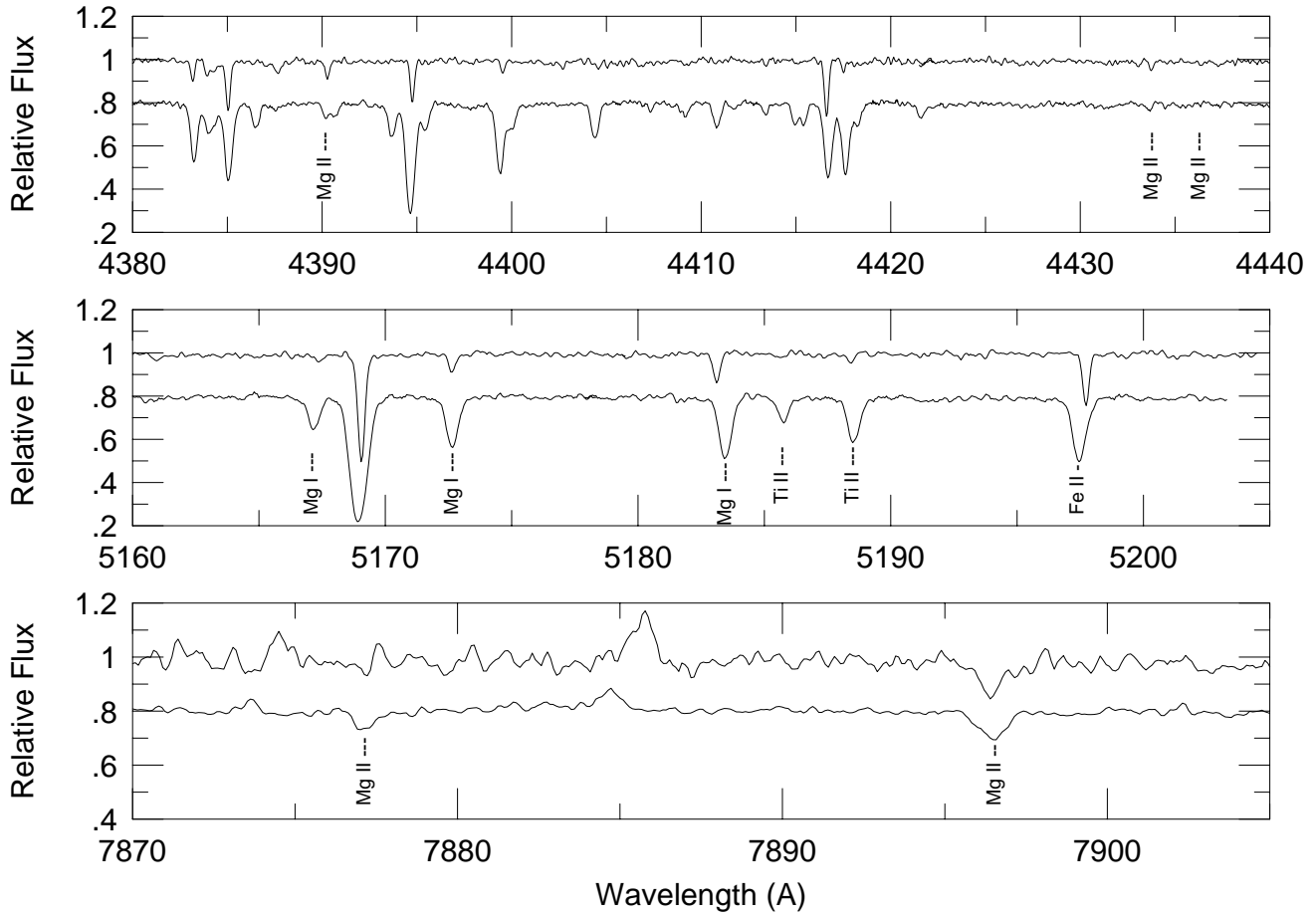


Fig. 4.— Sample spectra of AV 298 (upper) and AV 442 (lower) to show some Mg I and Mg II lines used for atmospheric parameter and abundance determinations. Spectra at 7900 Å have been divided by that of a hotter, rapidly-rotating star to remove telluric features.

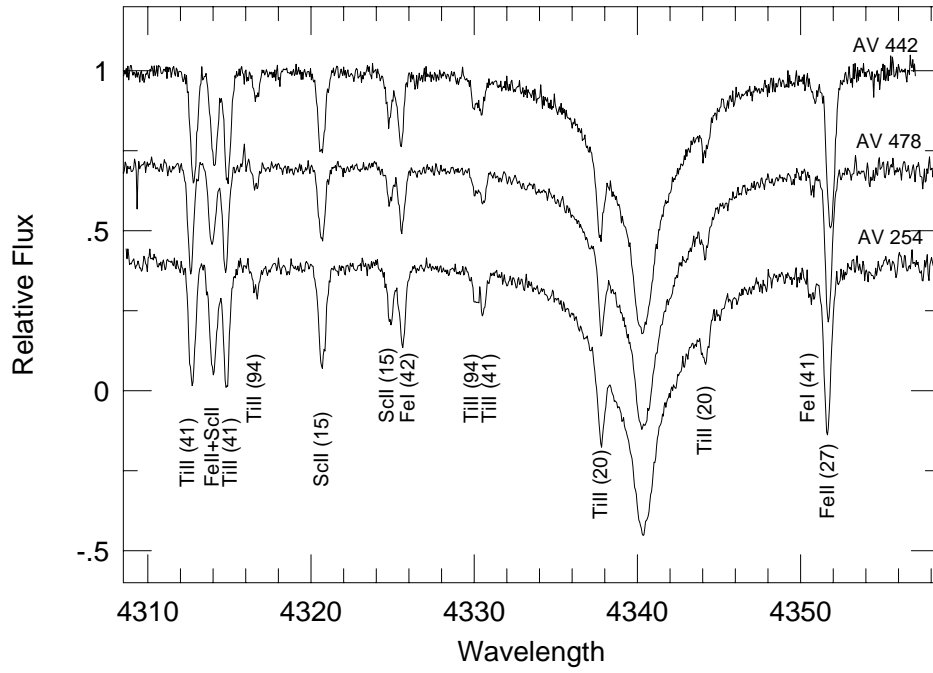


Fig. 5.— Spectra of three SMC A7Iab supergiants around  $H\gamma$ . Previously, AV 442 had been reported as a normal A3 Ia star, while the other two were reported as “anomalous”, helium-rich A3 I stars partially based on a comparison of their hydrogen line profiles (Humphreys 1983, et al. 1991).

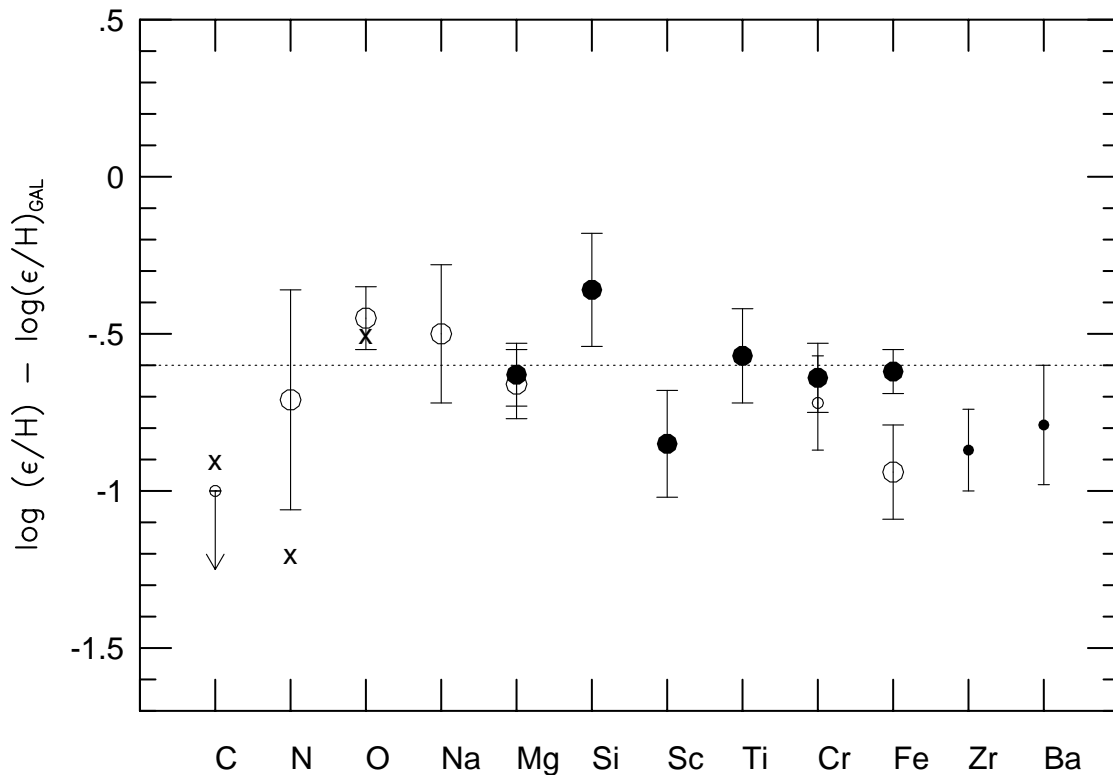


Fig. 6.— The average abundances of SMC A-type supergiants relative to Galactic A-type supergiants. Exceptions include Na, Zr, and Ba, which are relative to solar abundances (from Anders & Grevesse 1989) since these elements are not well determined in the Galactic stars. Abundances from ions (*filled circles*) and neutrals (*hollow circles*) are noted separately; also, the size of the data points are related to the number of stars used in each average. The mean depletion of the metals ( $\sim 0.6$  dex) is noted by the dotted line. X's mark the SMC nebular abundances for CNO.

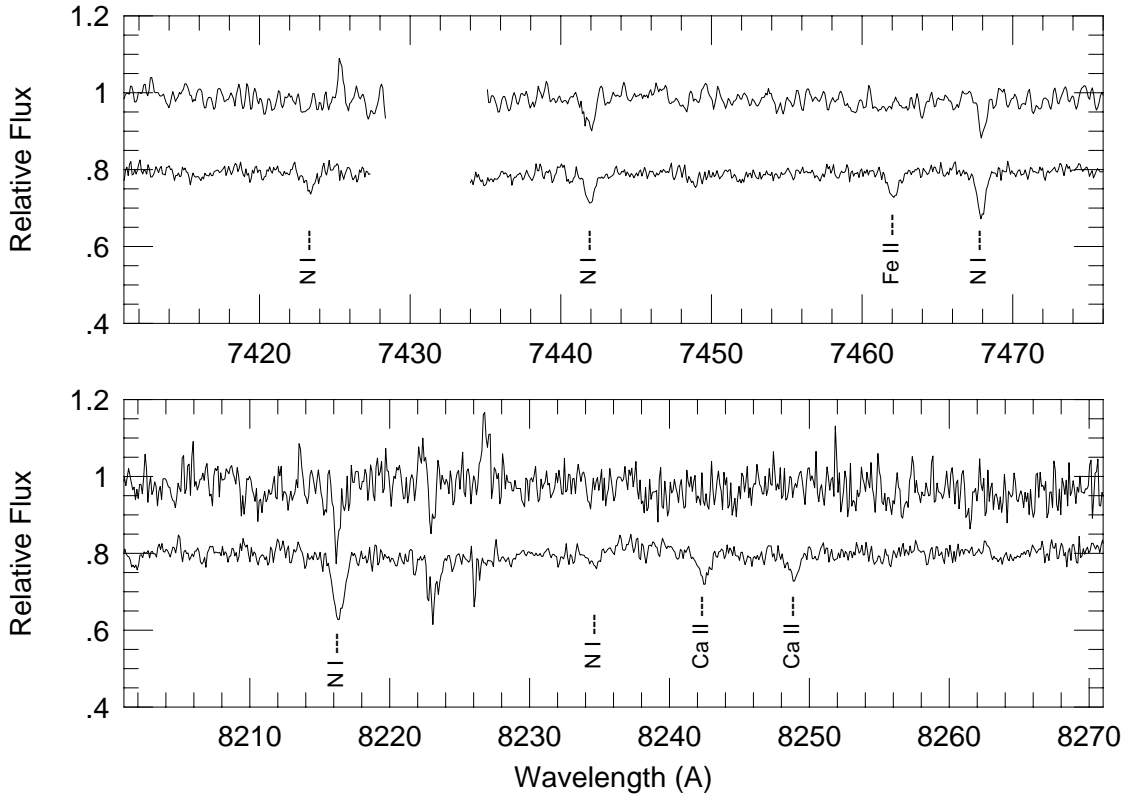


Fig. 7.— Sample spectra of AV 298 (upper) and AV 442 (lower) to show N I lines. Spectra at 8200 Å have been divided by that of a hotter, rapidly-rotating star to remove telluric features.

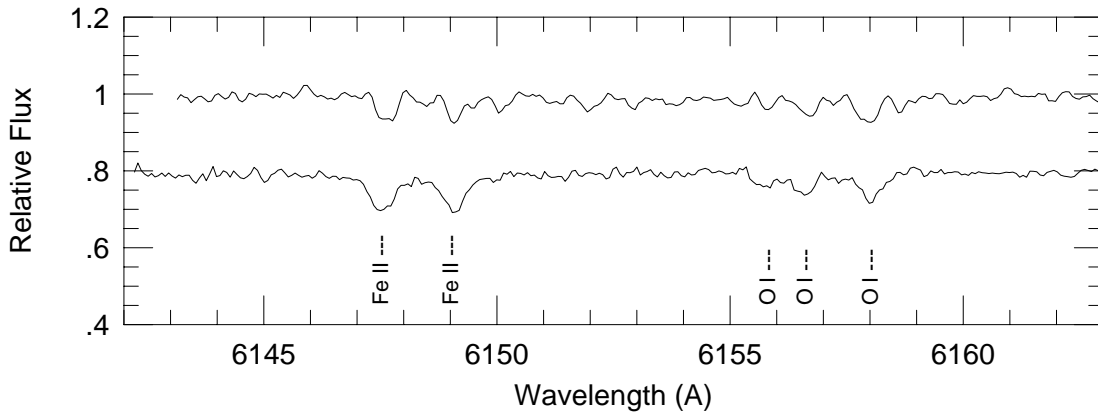


Fig. 8.— Sample spectra of AV 298 (upper) and AV 442 (lower) to show O I lines.

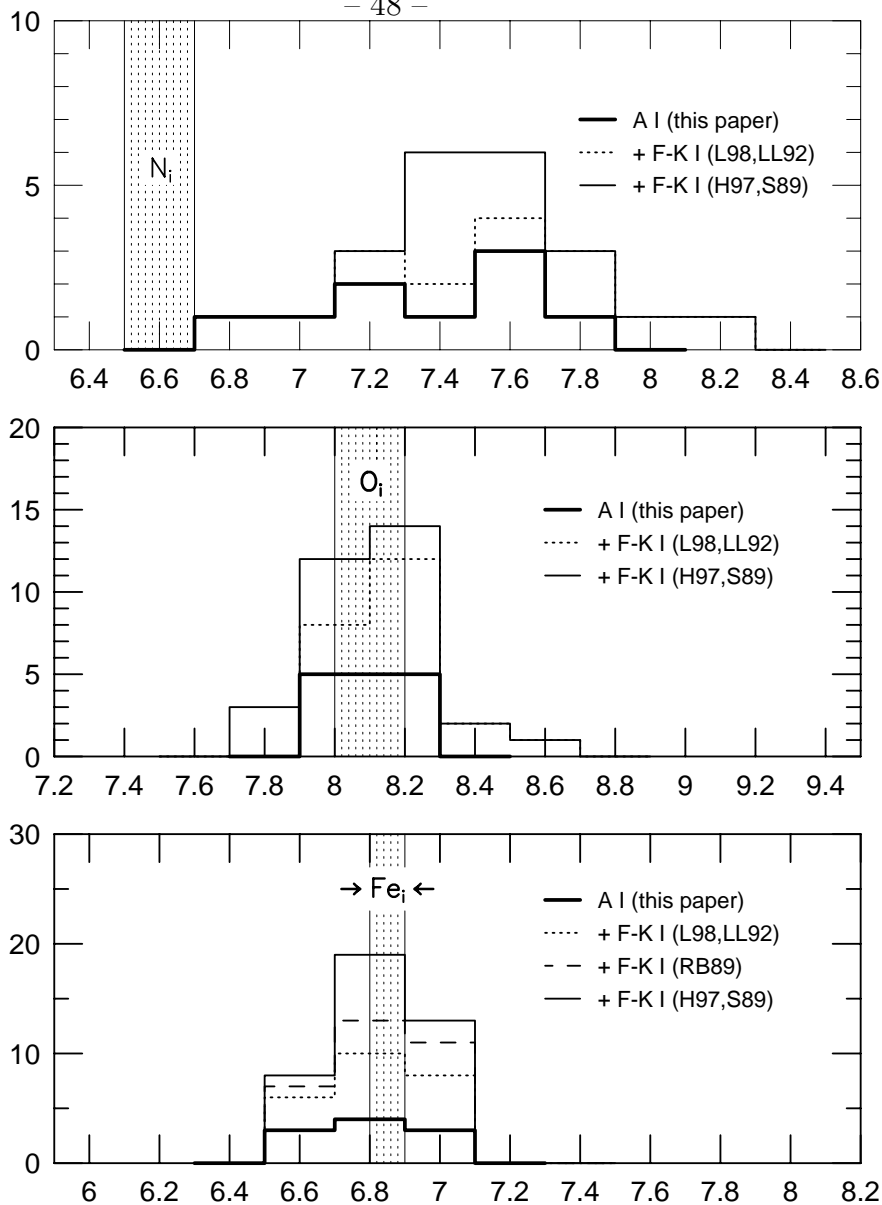


Fig. 9.— Histograms of the N, O, and Fe abundances in A- to K-type supergiants in the SMC. The A-supergiant abundances (this paper) are graphed by a thick, solid line, and the F-K supergiant abundances (see text for references) are added on top for clarity. Initial, present-day, abundances are noted as grey regions. Notice that the range in N is much larger than O or Fe.



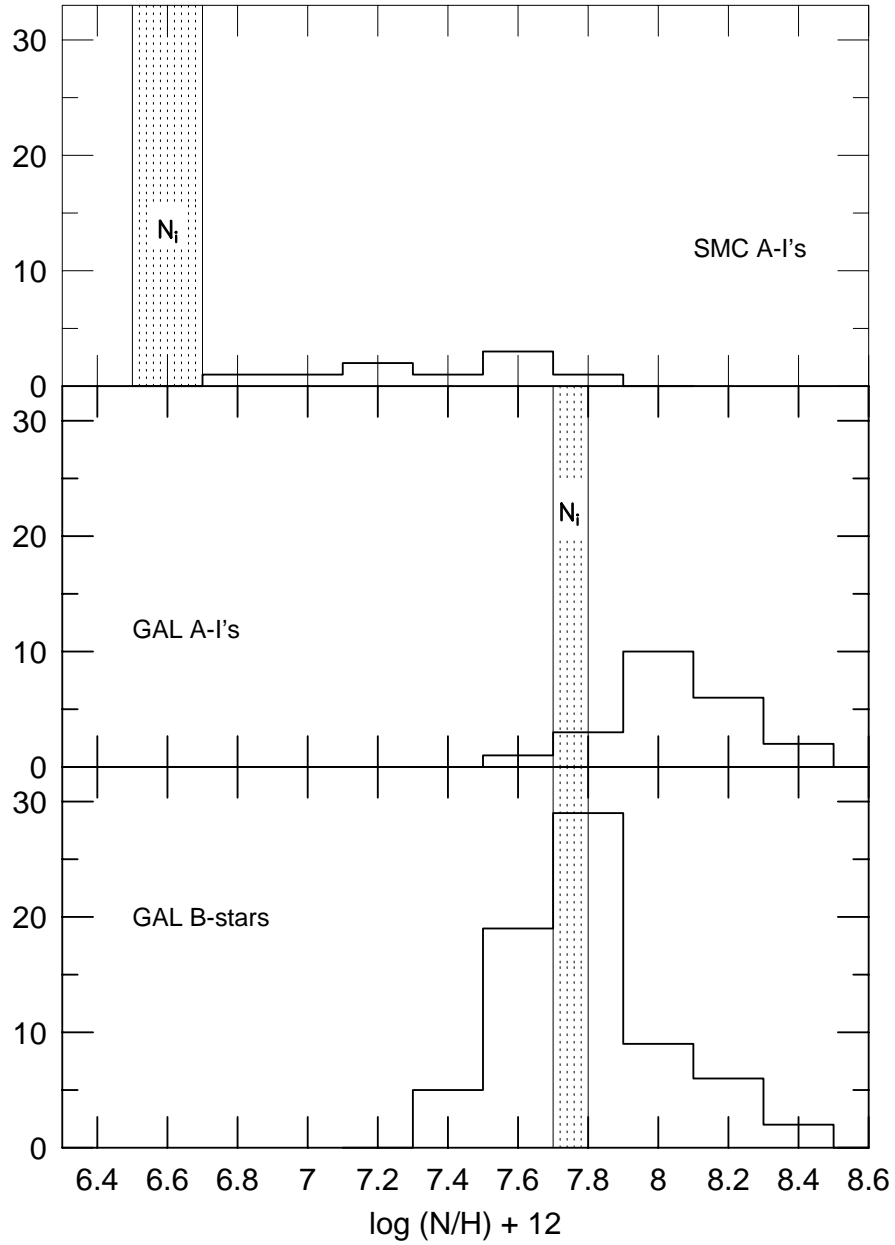


Fig. 10.— Distribution of nitrogen abundances in the SMC and Galactic A-supergiants, and Galactic B-stars (see text for references). The initial abundances are marked. Notice that the SMC stars are more enriched in N overall, and yet some stars show very little enrichment.

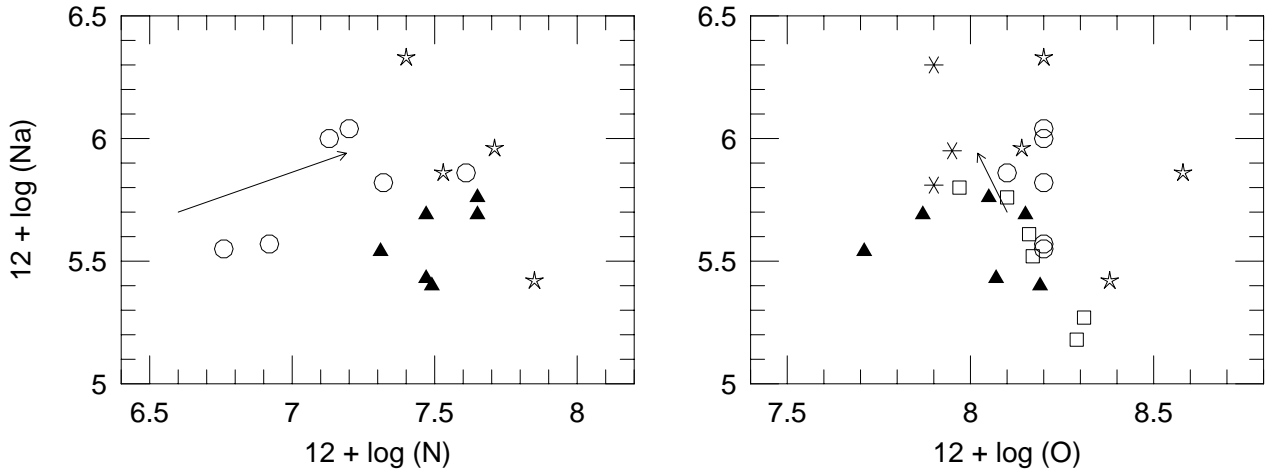


Fig. 11.— Comparison of Na with N and O determinations in SMC supergiants. No statistically significant trends are found, suggesting that Na enrichments are not related to mixing of Ne-Na cycled gas, which would be accompanied by CNO-cycled gas. Data is from this paper (*open circles*), Luck et al. (1998, *open squares*), Luck & Lambert (1992, *stars*), Hill (1997a,b, *filled triangles*), and Spite et al. (1989a,b, *asterisks*). Arrows indicate predicted first dredge-up abundances for classical non-rotating stellar evolution models (Heger 1998).

Table 1: SMC A-Type Supergiant Parameters

AV	Sk	Sp.Ty	Sp.Ty	V	$T_{\text{eff}}$	log g	Velocities ( $\text{km s}^{-1}$ )		
		OLD	NEW				$\xi$	$v_{\text{rad}}$	$v \sin i$
AV 110	Sk 49	A0 Ia	A1 Ia	12.1	9500	1.4	4	+160	25
AV 298		A0 Iab	A1 Ia	12.5	9400	1.7	3	+155	15
AV 392	Sk 125	A3 Ib	A3 Ib	12.5	8500	1.7	3	+135	25
AV 136	Sk 54	A0 Ia	A5 Iab	11.0	8200	1.0	6	+160	20
AV 463	Sk 146	A2 Ib	A7 Ib	12.2	8000	1.3	4	+170	25
AV 478	Sk 154	A0 Ib	A7 Iab	11.6	8100	1.1	5	+180	15
AV 254	Sk 89	A2 Ib	A7 Iab	11.6	8000	1.1	6	+180	20
AV 442	Sk 136	A3 Iab	A7 Iab	11.4	7900	0.9	7	+185	20
AV 213	Sk 75	A2 Iab	F0 Ia	12.0	7500	0.5	6	+175	20
AV 174	Sk 63	A7 Iab	F2 Iab	12.4	7200	0.8	4	+165	35

Table 2: Atmospheric Parameter Uncertainties

Star	H $\gamma$ fits		Mg I = Mg II $\pm$ 0.2		LTE Mg $\pm$ 0.2	
	$\Delta T_{\text{eff}}$	$\Delta \log g$	$\Delta T_{\text{eff}}$	$\Delta \log g$	$\Delta T_{\text{eff}}$	$\Delta \log g$
AV 110	$\pm 200$	$\pm 0.1$	$\pm 250$	$\pm 0.2$	<i>+250</i>	<i>+0.2</i>
AV 298	$\pm 200$	$\pm 0.1$	$\pm 200$	$\pm 0.2$	<i>+200</i>	<i>+0.1</i>
AV 392	$\pm 200$	$\pm 0.1$	$\pm 200$	$\pm 0.2$	<i>+200</i>	<i>+0.1</i>
AV 136	$\pm 100$	$\pm 0.1$	$\pm 100$	$\pm 0.2$	<i>+300</i>	<i>+0.1</i>
AV 463	$\pm 100$	$\pm 0.1$	$\pm 100$	$\pm 0.2$	<i>+200</i>	<i>+0.2</i>
AV 478	$\pm 100$	$\pm 0.1$	$\pm 150$	$\pm 0.2$	<i>+100</i>	<i>0.0</i>
AV 254	$\pm 100$	$\pm 0.1$	$\pm 150$	$\pm 0.2$	<i>+100</i>	<i>0.0</i>
AV 442	$\pm 100$	$\pm 0.1$	$\pm 150$	$\pm 0.2$	<i>+100</i>	<i>0.0</i>
AV 213	$\pm 100$	$\pm 0.1$	$\pm 100$	$\pm 0.2$	<i>+300</i>	<i>+0.2</i>
AV 174	$\pm 200$	$\pm 0.2$	$\pm 250$	$\pm 0.2$	<i>+250</i>	<i>+0.2</i>

TABLE 3  
ELEMENTAL ABUNDANCES

Elem	AV 110	AV 298	AV 392	AV 136	AV 463
C I	< 8.7	< 8.4	< 8.1	< 8.2	< 7.8
N I NLTE	7.64 ±0.18 (4)	7.65 ±0.21 (3)	< 7.2	7.26 ±0.07 (5)	6.92 ±0.25 (3)
<i>N I LTE</i>	8.24 ±0.23	8.32 ±0.23	< 7.9	8.18 ±0.17	7.50 ±0.33
O I NLTE	8.1	8.1	8.2	8.1	8.2
<i>O I LTE</i>	8.4 ±0.2 (S)	8.4 ±0.1 (S)	8.4 (1)	8.3 ±0.2 (S)	8.4 ±0.2 (S)
Na I	...	...	6.04 (1)	...	5.57 ±0.04 (2)
Mg I NLTE	6.87 (1)	7.03 ±0.04 (3)	6.83 ±0.09 (4)	6.77 ±0.15 (4)	6.99 ±0.10 (3)
<i>Mg I LTE</i>	6.73	6.91 ±0.04	6.81 ±0.07	6.74 ±0.27	6.89 ±0.06
Mg II NLTE	6.80 ±0.01 (2)	6.97 ±0.18 (2)	6.83 (1)	6.82 ±0.13 (3)	7.02 ±0.02 (3)
<i>Mg II LTE</i>	6.89 ±0.22	7.16 ±0.50	7.19	6.97 ±0.26	7.07 ±0.18
Si II	7.21 ±0.12 (3)	6.96 ±0.29 (6)	7.26 ±0.27 (3)	7.22 ±0.08 (5)	6.86 ±0.06 (3)
Ca II	...	...	...	5.46 (1)	5.56 ±0.04 (2)
Sc II	...	...	2.42 (1)	2.28 ±0.07 (2)	2.34 (1)
Ti II	4.04 ±0.04 (3)	4.12 ±0.10 (16)	4.48 ±0.16 (22)	4.26 ±0.12 (28)	4.48 ±0.17 (32)
Cr I	...	...	...	...	5.21 ±0.09 (2)
Cr II	4.78 ±0.15 (8)	4.95 ±0.18 (16)	5.09 ±0.16 (12)	5.12 ±0.20 (15)	5.00 ±0.19 (15)
Fe I	...	6.67 ±0.11 (5)	6.63 ±0.15 (7)	6.54 ±0.19 (9)	6.68 ±0.18 (17)
Fe II	6.68 ±0.21 (26)	6.71 ±0.16 (33)	6.81 ±0.16 (19)	6.89 ±0.15 (37)	6.90 ±0.18 (33)
Sr II	...	...	1.46 ±0.10 (2)	1.32 ±0.14 (2)	1.35 ±0.19 (2)
Zr II	...	...	...	1.63 (1)	1.84 (1)
Ba II	...	...	...	...	1.56 (1)

TABLE 4  
ELEMENTAL ABUNDANCE UNCERTAINTIES

Elem	AV 110		AV 298		AV 392		AV 136		AV 463	
	$\Delta T_{\text{eff}}=$ +200 K	$\Delta \log g$ =-0.2	$\Delta T_{\text{eff}}=$ +200 K	$\Delta \log g$ =-0.2	$\Delta T_{\text{eff}}=$ +200 K	$\Delta \log g$ =-0.2	$\Delta T_{\text{eff}}=$ +100 K	$\Delta \log g$ =-0.2	$\Delta T_{\text{eff}}=$ +100 K	$\Delta \log g$ =-0.2
N I	+0.06	+0.12	+0.07	+0.11	...	...	+0.04	+0.05	+0.03	+0.04
O I	+0.06	+0.08	+0.05	+0.06	+0.04	+0.04	+0.02	+0.03	+0.01	+0.03
Na I	...	...	...	...	+0.20	+0.12	...	...	+0.14	+0.16
Si II	-0.02	-0.02	-0.02	-0.02	-0.02	-0.04	-0.02	+0.03	-0.02	+0.02
Mg I	+0.20	+0.20	+0.20	+0.19	+0.24	+0.12	+0.18	+0.18	+0.14	+0.18
Mg II	+0.01	+0.01	0.00	+0.01	0.00	0.00	0.00	+0.01	0.00	+0.01
Ca II	...	...	...	...	...	...	+0.29	+0.14	+0.18	+0.14
Sc II	...	...	...	...	+0.22	+0.05	+0.16	+0.10	+0.12	+0.09
Ti II	+0.16	+0.08	+0.16	+0.08	+0.16	+0.02	+0.12	+0.06	+0.09	+0.05
Cr II	+0.06	+0.02	+0.07	0.00	+0.08	0.00	+0.07	+0.02	+0.06	+0.02
Fe I	...	...	+0.17	+0.14	+0.26	+0.12	+0.22	+0.18	+0.14	+0.18
Fe II	+0.04	0.00	+0.05	-0.02	+0.10	0.00	+0.06	+0.01	+0.06	+0.01
Sr II	...	...	...	...	+0.30	+0.10	+0.23	+0.18	+0.17	+0.16
Zr II	...	...	...	...	...	...	+0.12	+0.06	+0.09	+0.04
Ba II	...	...	...	...	...	...	...	...	+0.18	+0.18

TABLE 5  
ELEMENTAL ABUNDANCES

Elem	AV 478	AV 254	AV 442	AV 213	AV 174
C I	< 7.9	< 7.8	< 7.9	< 7.6	< 7.3
N I NLTE	7.61 ±0.16 (4)	7.13 ±0.27 (2)	7.32 ±0.21 (4)	7.74 ±0.22 (5)	6.76 (1)
<i>N I LTE</i>	<i>8.43 ±0.24</i>	<i>7.84 ±0.36</i>	<i>8.07 ±0.26</i>	<i>8.36 ±0.30</i>	<i>7.07</i>
O I NLTE	8.1	8.2	8.2	8.0	8.2
<i>O I LTE</i>	<i>8.3 ±0.1 (S)</i>	<i>8.4 ±0.1 (S)</i>	<i>8.4 ±0.1 (4)</i>	<i>8.1 ±0.1 (S)</i>	<i>8.3 ±0.2 (S)</i>
Na I	5.86 ±0.21 (3)	6.00 (1)	5.82 (1)	...	5.55 (1)
Mg I NLTE	6.76 ±0.07 (4)	6.79 ±0.08 (3)	6.72 ±0.11 (3)	6.78 ±0.05 (2)	6.69 (1)
<i>Mg I LTE</i>	<i>6.70 ±0.08</i>	<i>6.71 ±0.06</i>	<i>6.62 ±0.10</i>	<i>6.66 ±0.05</i>	<i>6.65</i>
Mg II NLTE	6.83 ±0.07 (4)	6.84 ±0.13 (4)	6.71 ±0.03 (3)	6.77 ±0.10 (2)	6.74 (1)
<i>Mg II LTE</i>	<i>6.90 ±0.16</i>	<i>6.89 ±0.04</i>	<i>6.73 ±0.20</i>	<i>6.86 ±0.01</i>	<i>6.97</i>
Si II	6.88 ±0.13 (4)	6.79 ±0.12 (4)	6.71 ±0.06 (5)	6.94 ±0.14 (4)	6.91 ±0.16 (2)
Ca I	5.26 (1)	5.31 (1)	5.26 (1)	5.20 (1)	5.97 ±0.15 (5)
Ca II	...	5.31 ±0.25 (2)	5.21 ±0.05 (2)	5.40 ±0.35 (2)	5.38 (1)
Sc II	2.12 ±0.27 (4)	2.28 ±0.07 (3)	2.22 ±0.15 (4)	2.22 ±0.19 (3)	2.27 ±0.18 (3)
Ti II	4.33 ±0.19 (35)	4.39 ±0.20 (35)	4.28 ±0.19 (35)	4.25 ±0.22 (28)	4.31 ±0.26 (21)
Cr I	...	...	...	5.04 ±0.11 (3)	5.25 ±0.26 (4)
Cr II	4.93 ±0.13 (17)	4.99 ±0.16 (18)	4.87 ±0.18 (17)	4.90 ±0.18 (15)	5.06 ±0.23 (13)
Fe I	6.46 ±0.17 (10)	6.58 ±0.19 (15)	6.52 ±0.22 (15)	6.61 ±0.22 (23)	6.89 ±0.17 (22)
Fe II	6.80 ±0.16 (31)	6.80 ±0.16 (31)	6.71 ±0.14 (30)	6.71 ±0.16 (24)	6.86 ±0.23 (25)
Sr II	1.09 ±0.07 (2)	1.20 ±0.07 (2)	1.07 ±0.08 (2)	1.00 (1)	...
Zr II	1.65 (1)	1.72 (1)	1.75 (1)	1.62 (1)	1.94 ±0.10 (2)
Ba II	1.40 (1)	1.31 (1)	1.24 (1)	1.34 ±0.25 (2)	1.66 (1)

TABLE 6  
ELEMENTAL ABUNDANCE UNCERTAINTIES

Elem	AV 478		AV 254		AV 442		AV 213		AV 174	
	$\Delta T_{\text{eff}} =$ +150 K	$\Delta \log g$ =-0.2	$\Delta T_{\text{eff}} =$ +150 K	$\Delta \log g$ =-0.2	$\Delta T_{\text{eff}} =$ +150 K	$\Delta \log g$ =-0.2	$\Delta T_{\text{eff}} =$ +100 K	$\Delta \log g$ =-0.2	$\Delta T_{\text{eff}} =$ +200 K	$\Delta \log g$ =-0.2
N I	+0.08	+0.04	+0.06	+0.06	+0.07	+0.10	+0.04	+0.06	+0.01	+0.02
O I	+0.05	+0.02	+0.04	+0.05	+0.06	+0.08	+0.03	+0.04	+0.06	+0.04
Na I	+0.26	+0.17	+0.26	+0.21	+0.30	+0.28	+0.19	+0.25	+0.22	+0.13
Mg I	+0.26	+0.18	+0.26	+0.21	+0.29	+0.30	+0.20	+0.25	+0.23	+0.14
Mg II	0.00	0.00	+0.02	+0.03	+0.02	+0.02	+0.02	+0.03	0.00	0.00
Si II	-0.02	-0.02	-0.02	-0.01	-0.03	0.00	+0.01	+0.04	-0.01	-0.01
Ca II	+0.22	+0.13	+0.19	+0.17	+0.22	+0.28	+0.16	+0.20	+0.12	+0.08
Sc II	+0.24	+0.08	+0.23	+0.12	+0.27	+0.18	+0.17	+0.13	+0.19	+0.04
Ti II	+0.19	+0.05	+0.17	+0.08	+0.19	+0.14	+0.13	+0.10	+0.16	+0.02
Cr II	+0.11	+0.02	+0.11	+0.04	+0.14	+0.08	+0.09	+0.08	+0.11	+0.02
Fe I	+0.29	+0.18	+0.29	+0.22	+0.32	+0.30	+0.26	+0.26	+0.27	+0.14
Fe II	+0.11	+0.02	+0.11	+0.04	+0.12	+0.08	+0.09	+0.07	+0.13	+0.01
Sr II	+0.34	+0.16	+0.33	+0.21	+0.37	+0.30	+0.26	+0.25	...	...
Zr II	+0.18	+0.04	+0.17	+0.07	+0.29	+0.14	+0.15	+0.11	+0.18	+0.03
Ba II	+0.35	+0.17	+0.34	+0.22	+0.37	+0.32	+0.27	+0.27	+0.35	+0.13

Table 7: SMC and Galactic A-Type Supergiant Abundances (Relative to Solar)

Elem	SUN	SMC AIs AVER $\pm\sigma$ (#)	SMC AIs [M/H]	Galactic AIs [M/H] (N)
N I	7.8 <sup>a</sup>	7.33 $\pm$ 0.35 ( 9)	-0.47 <sup>a</sup>	+0.25 (22)
O I	8.6 <sup>a</sup>	8.14 $\pm$ 0.10 ( 9)	-0.46 <sup>a</sup>	-0.01 <sup>b</sup> (22)
Na I	6.31	5.81 $\pm$ 0.22 ( 6)	-0.50	+0.66 (11)
Mg I	7.58	6.82 $\pm$ 0.11 (10)	-0.76	-0.10 (19)
Mg II	7.58	6.83 $\pm$ 0.10 (10)	-0.75	-0.12 (22)
Si II	7.55	6.97 $\pm$ 0.18 (10)	-0.58	-0.22 ( 5)
Ca I	6.34	5.23 $\pm$ 0.14 ( 4)	-1.11	+0.31 (15)
Ca II	6.34	5.39 $\pm$ 0.16 ( 6)	-0.95	-0.31 (10)
Sc II	3.09	2.28 $\pm$ 0.17 ( 8)	-0.81	+0.04 ( 9)
Ti II	4.93	4.29 $\pm$ 0.15 (10)	-0.64	-0.07 (22)
Cr I	5.68	5.17 $\pm$ 0.15 ( 3)	-0.51	+0.21 ( 8)
Cr II	5.68	4.97 $\pm$ 0.11 (10)	-0.71	-0.07 (18)
Fe I	7.51	6.62 $\pm$ 0.15 ( 9)	-0.89	+0.05 (22)
Fe II	7.51	6.78 $\pm$ 0.07 (10)	-0.73	-0.11 (22)
Sr II	2.93	1.21 $\pm$ 0.19 ( 7)	-1.72	-0.52 ( 4)
Zr II	2.61	1.74 $\pm$ 0.13 ( 7)	-0.87	+0.20 ( 3)
Ba II	2.21	1.42 $\pm$ 0.19 ( 6)	-0.79	...

<sup>a</sup>Note that solar neighbourhood abundances are adopted for these elements (discussed in Section 6.1, also see Table 9).

<sup>b</sup>The same NLTE corrections applied to the SMC O I abundances have been applied here to the Galactic A-supergiant LTE abundances from Venn (1995a).

Table 8: Differential (“like – like”) Abundances for SMC Stars

Elem	Solar Neigh.	A Is <sup>a</sup> ( $\leq 10$ stars)	LL92 <sup>b</sup> ( $\leq 7$ stars)	RB89 <sup>c</sup> ( $\leq 8$ stars)	S89 <sup>c</sup> ( $\leq 3$ stars)	H97 <sup>d,g</sup> ( $\leq 6$ stars)	L98 <sup>e</sup> ( $\leq 6$ stars)	IIIIs <sup>f</sup> ( $\leq 6$ stars)
C	8.3	...	-0.6	-0.5	-0.7	-0.8	-0.7	< -0.4
N	7.8	-0.8	-0.9	...	...	-0.3	...	> -0.9
O	8.6	-0.5	-0.4	...	-0.6	-0.7	-0.7	-0.6
Na	6.3	-1.1	-0.9	-0.4	-0.7	-0.7	-1.0	...
Mg	7.6	-0.7	-0.5	-0.6	-0.7	-0.5	-0.8	-0.6
Si	7.6	-0.3	-0.4	...	-0.5	-0.8	-0.8	-0.9
Ca	6.3	-0.6	-0.5	-0.2	-0.6	-0.8	-0.6	...
Sc	3.1	-0.8	-0.4 <sup>g</sup>	-0.5	-0.6	-0.9	-0.9	...
Ti	4.9	-0.7	-0.6	-0.5	-0.8	-0.7	-0.7	...
Cr	5.7	-0.6	-0.4 <sup>g</sup>	-0.4	-0.6	-1.0	-0.7	...
Fe I	7.5	-0.9	-0.6	-0.5	-0.6	-0.7	-0.7	...
Fe II	7.5	-0.6	-0.6	-0.6	-0.6	-0.7	-0.7	...
Sr	2.9	-1.2	...	-1.4	...	...	...	...
Zr	2.6	-1.0	...	-0.6	-0.5	...	-0.9	...
Ba	2.2	-0.8 <sup>g</sup>	...	-0.9	-0.6	...	...	...

<sup>a</sup> A Is = SMC (this paper) minus Galactic (Venn 1995a,b) A-supergiant abundances.

<sup>b</sup> LL92 = SMC (Luck & Lambert 1992) minus Galactic (Luck & Lambert 1985) F-K supergiant abundances.

<sup>c</sup> RB89, S89 = SMC F-G supergiants (Russell & Bessell 1989, Spite et al. 1989a,b) minus Canopus abundances.

<sup>d</sup> H97 = SMC K supergiant (Hill et al. 1997a,b) minus solar abundances (their comparison star, Arcturus, is metal-poor with  $[\text{Fe}/\text{H}] = -0.5$ ).

<sup>e</sup> L98 = SMC F-K supergiant and Cepheid (Luck et al. 1998) minus Galactic F-K supergiant (Luck et al. 1998) abundances.

<sup>f</sup> IIIIs = mean of 6 differential B-giant abundances:

- (1) IDK-D2 minus 67 Oph (Rolleston et al. 1993),
- (2) AV175, NGC330-B30, NGC330-B22 minus HR 2618 (Jüttner et al. 1992),
- (3) NGC330-B30 minus HR 3663 (Reitermann et al. 1991),
- (4) NGC330-A01, NGC330-B04 (Lennon et al. 1996) relative to  $\tau$  Sco (from Rolleston et al. 1993).

<sup>g</sup> Abundances that are relative to the solar neighborhood (column 1) and not the comparison stars.

Table 9: Galactic Nebular and B-Star Abundances

Elem	SUN	Orion							B-stars			Adopted
		D84	B91	R91	O92	W92 0/0.055 <sup>a</sup>	P93 0/0.04 <sup>a</sup>	E98 g/g+d <sup>b</sup>	GL	K	CL	
C	8.6	8.2	8.3	8.5*	8.6	7.9/8.8	8.5/8.5	8.4/8.5	8.2	8.2	8.4	8.3
N	8.0	7.5	7.9	7.8	7.6	7.5/7.7	7.7/7.9	7.8/7.8	7.8	7.8	7.8	7.8
O	8.9	8.7	8.6	8.6	8.5	8.4/8.9	8.5/8.8	8.6/8.7	8.7	8.6	8.6	8.6

D84 = Dufour 1984, B91 = Baldwin et al. 1991, R91 = Rubin et al. 1991 (\* Same C in Rubin et al 1993), O92 = Osterbrock et al. 1992, W92 = Walter et al. 1992, P93 = Peimbert et al. 1993, E98 = Esteban et al. 1998, GL = Gies & Lambert 1992, K = Kilian 1992, CL = Cunha & Lambert 1994. Solar abundances from Anders & Grevesse 1989, Grevesse & Noels 1993.

<sup>a</sup> Different abundances depend on the estimated temperature fluctuations as 0%, 5.5%, or 4%.

<sup>b</sup> Abundances from nebular gas measurements only (g), and those corrected for dust depletions (g+d).

Table 10: SMC Nebular and B-Star Abundances

Elem	Nebulae				GAL	B-stars		Adopted
	D84	RD90	G95	K98		R93	( = )	
C	7.2	...	7.4	7.5	8.3	-0.9	( 7.4 )	7.4
N	6.5	6.6	6.3	6.6	7.8	<-1.1	(<6.7)	6.6
O	8.0	8.1	8.1	8.1	8.6	-0.5	( 8.1 )	8.1

D84 = Dufour 1984, RD90 = Russell & Dopita 1990, G95 = Garnett et al. 1995, K98 = Kurt et al. 1998, R93 = Rolleston et al. 1993. Note that the B-stars/nebular C abundance is 0.3 dex less than that reported from F-K supergiants (see discussion in text).



TABLE 11  
LINE DATA AND EQUIVALENT WIDTHS

Elem	Mult	Wavel	$\chi$	log gf	Comm	110	298	392	136	463	478	254	442	213	174
700	3	7423.63	10.33	-0.69	zhu	...	...	...	31	...	79	...	58	90	...
700	3	7442.28	10.33	-0.40	zhu	48	57	...	66	...	90	...	64	150	...
700	3	7468.29	10.34	-0.21	zhu	78	65	...	105	80	134	80	85	...	...
700	2	8210.64	10.33	-0.68	zhu	...	...	...	58	...	22	...	...	94	...
700	2	8216.28	10.34	0.09	zhu	75	96	...	190	60	175	109	179	...	54
700	2	8223.07	10.33	-0.29	zhu	...	...	...	167	46	...	...	...	...	...
700	2	8242.34	10.34	-0.26	zhu	55	...	...	105	...	116	...	77	154	...
800	10	6155.99	10.74	-0.67	op	14	...	...	...	...	...	...	27	...	...
800	10	6156.78	10.74	-0.45	op	16	...	...	...	...	36	...	32	...	...
800	10	6158.19	10.74	-0.31	op	36	36	...	57	53	40	74	45	38	...
800	9	6454.48	10.74	-1.14	op	...	...	...	...	...	...	...	17	...	...
1100	1	5889.95	0.00	0.11	wm	...	...	...	...	131	125	235	189	...	...
1100	1	5895.92	0.00	-0.19	wm	...	...	...	...	105	93	157	126	...	...
1100	4	8194.82	2.10	0.51	wm	...	...	50	...	...	63	...	...	156	110
1200	11	4702.98	4.35	-0.37	wm	...	10	25	20	50	13	24	16	40	97
1200	2	5167.32	2.71	-0.86	wm	...	13	64	60	130	79	100	88	130	...
1200	2	5172.68	2.71	-0.38	wm	20	29	97	74	160	118	155	137	...	...
1200	2	5183.60	2.72	-0.16	wm	36	46	124	92	202	148	184	180	...	...
1201	10	4390.59	10.00	-0.53	wsm	...	24	...	...	...	31	...	...	...	...
1201	9	4427.99	10.00	-1.21	wsm	...	...	11	...	19	...	11	...	...	...
1201	9	4433.99	10.00	-0.91	wsm	...	...	15	...	21	...	13	21	18	...
1201	19	4436.48	11.57	-0.89	wsm	...	10	...	...	...	...	...	...	...	...
1201	8	7877.13	10.00	0.39	wsm	...	51	50	91	...	38	...	49	42	...
1201	8	7896.37	10.00	0.65	wsm	100	90	100	150	142	100	86	102	110	98
1401	3	4128.05	9.84	0.31	wm	135	66	...	...	...	103	...	103	127	...
1401	3	4130.88	9.84	0.46	wm	152	91	...	145	92	100	93	102	128	...
1401	5	5041.06	10.07	0.17	nk	101	59	65	103	53	59	57	52	55	...
1401	5	5056.02	10.08	0.59	nk	...	72	82	153	79	103	85	...	96	69
1401	4	5957.61	10.07	-0.35	wm	47	...	...	39	...	...	...	...	...	...
1401	4	5978.97	10.07	-0.06	wm	70	...	...	62	...	...	...	28	...	...
1401	2	6347.09	8.12	0.23	wm	...	146	...	...	...	...	...	...	...	...
1401	2	6371.36	8.12	-0.08	wm	...	126	145	...	...	...	204	...	...	150
2000	2	4226.73	0.00	0.24	wm	...	...	...	...	...	45	75	59	119	...
2000	4	4425.44	1.88	-0.39	wm	...	...	...	...	...	...	...	...	...	58
2000	4	4435.30	1.89	0.00	wm	...	...	...	...	...	...	...	...	...	130
2000	3	6162.17	1.90	-0.09	wm	...	...	...	...	...	...	...	...	...	116
2000	18	6439.07	2.53	0.47	wm	...	...	65	...	...	...	...	...	...	...
2000	18	6462.57	2.52	0.31	wm	...	...	139	...	...	...	...	...	...	73
2000	30	7148.15	2.71	0.00	wm	...	...	...	...	...	...	...	...	...	52
2001	13	8203.20	7.51	0.30	wsm	...	...	...	...	116	...	39	39	...	165
2001	13	8250.20	7.52	0.57	wsm	...	...	...	61	142	55	117	76	100	...
2001	13	8256.10	7.52	-0.40	wsm	...	...	...	...	62	...	...	...	42	48
2101	8	4014.49	0.32	-1.66	nk	...	...	...	...	...	...	15	15	48	89
2101	7	4246.83	0.32	0.32	nk	...	18	85	...	175	142	198	200:	...	...
2101	15	4305.72	0.60	-1.21	nk	...	...	17	...	...	...	...	...	...	...
2101	15	4320.75	0.61	-0.26	nk	...	...	76	75	...	119	170	150	...	...
2101	15	4325.01	0.60	-0.44	nk	...	...	...	...	...	43	91	73	142	...
2101	14	4420.66	0.62	-2.03	nk	...	...	...	...	...	...	...	...	...	19

TABLE 11—*Continued*

Elem	Mult	Wavel	$\chi$	log gf	Comm	110	298	392	136	463	478	254	442	213	174
2101	23	5031.02	1.36	-0.34	nk	...	...	...	20	55	...	50	35	79	119
2201	11	4012.37	0.57	-1.61	mfw	...	24	105	110	159	...	178	161	...	...
2201	11	4025.14	0.61	-1.98	mfw	...	...	...	...	...	...	102	82	163	...
2201	87	4028.33	1.89	-1.00	mfw	...	18	66	86	122	100	145	130	...	...
2201	87	4053.81	1.89	-1.21	mfw	...	...	69	92	121	...	142	122	...	...
2201	87	4053.83	1.89	-1.21	mfw	...	...	...	...	...	95	...	...	...	...
2201	21	4161.53	1.08	-2.36	mfw	...	...	...	...	...	54	...	55	...	...
2201	105	4163.60	2.59	-0.40	mfw	...	16	96	105	137	121	155	151	...	...
2201	105	4171.90	2.60	-0.56	mfw	...	20	80	97	142	...	152	139	...	...
2201	33	4227.34	1.13	-2.36	mfw	...	...	...	...	...	34	44	42	75	...
2201	20	4287.89	1.08	-2.02	mfw	...	...	60	53	101	68	96	91	145	...
2201	41	4290.22	1.16	-1.12	mfw	...	26	120	135	...	194	...	...	...	...
2201	20	4294.10	1.08	-1.11	mfw	...	37	105	130	...	187	...	...	...	...
2201	41	4300.05	1.18	-0.77	mfw	30	51	151	170	...	...	...	...	...	...
2201	41	4301.93	1.16	-1.16	mfw	...	19	...	91	...	129	173	159	...	...
2201	41	4307.90	1.16	-1.29	mfw	...	29	111	105	...	165	203	194	...	...
2201	41	4312.86	1.18	-1.16	mfw	...	27	82	86	161	140	192	178	...	...
2201	41	4314.98	1.16	-1.13	mfw	...	21	...	...	...	150	183	183	...	...
2201	94	4316.81	2.05	-1.42	mfw	...	...	21	...	...	29	44	36	62	110
2201	41	4320.97	1.16	-1.87	mfw	...	...	...	62	...	...	...	...	...	...
2201	104	4367.66	2.59	-1.27	mfw	...	...	...	...	...	54	68	56	114	...
2201	104	4386.86	2.60	-1.26	mfw	...	...	...	35	58	47	70	52	103	114
2201	51	4394.06	1.22	-1.59	mfw	...	...	...	...	...	54	88	78	155	...
2201	19	4395.03	1.08	-0.66	mfw	24	52	...	...	...	...	...	...	...	...
2201	61	4395.85	1.24	-2.17	mfw	...	...	...	...	...	58	65	71	...	...
2201	51	4399.77	1.24	-1.27	mfw	...	17	...	93	...	128	186	164	...	...
2201	51	4407.68	1.22	-2.47	mfw	...	...	...	...	35	18	...	...	...	86
2201	115	4411.08	3.09	-1.06	mfw	...	...	...	30	52	50	61	54	91	98
2201	40	4417.72	1.16	-1.43	mfw	...	...	...	...	...	159	189	183	...	...
2201	93	4421.95	2.06	-1.77	mfw	...	...	...	...	45	27	34	36	60	140
2201	40	4441.73	1.18	-2.41	mfw	...	...	...	17	...	20	38	31	64	...
2201	19	4443.80	1.08	-0.70	mfw	...	39	155	137	...	...	...	...	...	...
2201	31	4444.56	1.12	-2.03	mfw	...	...	...	...	...	33	...	...	...	...
2201	19	4450.49	1.08	-1.45	mfw	...	21	70	60	134	94	133	114	...	...
2201	40	4464.46	1.16	-2.08	mfw	...	...	45	42	87	69	96	80	158	...
2201	31	4468.49	1.13	-0.60	mfw	...	43	158	149	...	...	...	...	...	...
2201	40	4470.86	1.16	-2.28	mfw	...	...	...	...	...	29	55	...	93	135
2201	115	4488.32	3.12	-0.82	mfw	...	...	...	...	71	55	75	74	117	...
2201	18	4493.53	1.08	-2.73	mfw	...	...	...	...	...	...	...	...	...	40
2201	31	4501.27	1.12	-0.75	mfw	...	36	121	...	...	192	...	...	...	...
2201	18	4518.30	1.08	-2.56	nk	...	...	...	...	40	...	...	...	...	90
2201	82	4529.47	1.57	-2.03	nk	...	...	...	35	69	45	61	51	98	...
2201	60	4544.00	1.24	-2.40	mfw	...	...	...	...	17	...	18	20	42	...
2201	50	4563.76	1.22	-0.96	mfw	22	30	130	125	...	192	...	...	...	...
2201	82	4571.97	1.57	-0.53	mfw	...	52	142	158	...	...	...	...	...	...
2201	60	4580.46	1.23	-2.79	mfw	...	...	...	...	...	...	...	...	...	104
2201	50	4589.96	1.24	-1.79	mfw	...	...	58	54	100	78	106	95	168	...
2201	49	4708.66	1.24	-2.21	mfw	...	...	...	...	44	19	27	20	52	83

TABLE 11—*Continued*

Elem	Mult	Wavel	$\chi$	log gf	Comm	110	298	392	136	463	478	254	442	213	174
2201	59	4719.52	1.24	-3.22	nk	...	...	...	...	...	...	...	...	...	34
2201	92	4779.99	2.05	-1.37	mfw	...	...	40	35	83	51	77	75	124	160
2201	17	4798.54	1.08	-2.43	mfw	...	...	...	...	22	...	...	...	...	85
2201	92	4805.11	2.06	-1.10	mfw	...	...	55	65	113	97	122	116	188	...
2201	114	4874.03	3.09	-0.79	mfw	...	...	...	21	...	37	52	48	78	128
2201	114	4911.21	3.12	-0.34	mfw	...	...	59	38	66	60	78	69	109	127
2201	113	5010.20	3.10	-1.34	nk	...	...	...	...	...	...	...	...	31	58
2201	71	5013.71	1.58	-1.94	nk	...	...	...	...	41	...	28	...	43	85
2201	113	5069.12	3.12	-1.39	mfw	...	...	...	13	...	...	...	...	...	67
2201	113	5072.30	3.12	-0.75	mfw	...	...	...	23	37	...	...	35	47	94
2201	86	5129.14	1.89	-1.39	mfw	...	...	...	27	76	852	81	69	105	130
2201	70	5154.06	1.57	-1.92	mfw	...	...	43	49	82	50	87	...	...	...
2201	86	5185.90	1.89	-1.35	mfw	...	...	47	...	70	44	...	56	106	130
2201	70	5188.70	1.58	-1.21	mfw	...	15	79	53	132	110	125	122	...	...
2201	103	5211.54	2.59	-1.36	nk	...	...	...	...	30	...	...	...	...	...
2201	70	5226.53	1.57	-1.30	mfw	...	...	...	...	...	67	...	...	...	...
2301	32	4023.39	1.80	-0.52	nk	...	...	...	...	57	...	...	...	86	...
2400	22	4371.28	1.00	-1.09	nk	...	...	...	...	...	...	...	...	...	42
2400	7	5204.52	0.94	-0.21	mfw	...	...	...	...	...	...	...	...	33	86
2400	7	5206.04	0.94	0.02	mfw	...	...	...	...	41	...	...	...	34	150
2400	7	5208.40	0.94	0.16	mfw	...	...	...	...	42	...	...	...	53	130
2401	162	4145.77	5.32	-1.16	nk	...	...	...	37	...	...	29	...	42	51
2401	162	4224.85	5.33	-1.06	nk	...	...	...	48	...	...	...	...	...	...
2401	31	4242.38	3.87	-1.17	sl	24	38	74	108	...	92	117	110	164	155
2401	31	4252.62	3.86	-1.86	sl	...	15	...	...	...	...	35	31	...	100
2401	31	4261.92	3.86	-1.34	sl	31	31	50	75	82	79	92	85	132	140
2401	31	4269.28	3.85	-2.02	sl	...	8	...	...	...	27	35	33	49	87
2401	31	4275.57	3.86	-1.47	sl	...	18	...	57	...	64	58	63	82	...
2401	31	4284.21	3.85	-1.70	sl	...	18	49	52	55	43	50	47	78	...
2401	39	4539.62	4.04	-2.53	mfw	...	...	...	...	...	...	...	...	...	37
2401	44	4555.02	4.07	-1.38	mfw	21	28	...	...	...	66	83	82	121	...
2401	44	4558.66	4.07	-0.66	mfw	68	79	123	...	...	189	...	...	...	...
2401	39	4565.78	4.04	-2.11	mfw	...	...	...	33	33	...	38	28	50	83
2401	44	4588.22	4.07	-0.63	mfw	49	68	109	179	151	152	174	177	...	...
2401	44	4592.09	4.07	-1.22	mfw	...	25	56	70	79	63	84	80	100	125
2401	44	4616.64	4.07	-1.36	mfw	...	18	54	70	60	59	75	55	102	116
2401	44	4618.83	4.07	-0.84	mfw	35	46	84	125	127	118	150	132	189	...
2401	44	4634.11	4.07	-0.96	mfw	...	35	...	...	89	92	116	108	158	142
2401	177	4697.62	5.67	-1.62	mfw	...	...	...	...	...	...	...	...	...	28
2401	30	4812.35	3.86	-1.80	mfw	...	...	21	31	36	24	35	24	40	62
2401	30	4824.12	3.87	-1.22	mfw	...	...	...	...	...	139	...	...	...	...
2401	30	4824.13	3.87	-1.22	mfw	42	53	95	138	133	...	155	156	...	...
2401	30	4836.22	3.86	-2.25	mfw	...	15	...	...	41	27	41	...	58	77
2401	30	4848.24	3.86	-1.14	mfw	31	45	81	115	118	...	148	134	179	...
2401	30	4858.24	3.86	-1.14	mfw	...	...	...	...	...	103	...	...	...	...
2401	30	4876.41	3.86	-1.46	mfw	...	...	65	89	100	88	110	110	145	...
2401	30	4884.58	3.86	-2.08	mfw	...	...	...	...	...	18	...	...	36	...
2501	5	4755.73	5.40	-1.24	nk	...	...	...	25	...	...	...	...	...	...

TABLE 11—*Continued*

Elem	Mult	Wavel	$\chi$	log gf	Comm	110	298	392	136	463	478	254	442	213	174
2600	4	3922.91	0.05	-1.65	fmw	...	...	...	...	73	...	...	...	...	...
2600	278	4021.87	2.76	-0.77	nk	...	...	...	...	...	...	...	...	...	78
2600	43	4045.82	1.48	0.28	ob	...	27	86	70	...	111	153	132	183	...
2600	43	4063.60	1.56	0.06	ob	...	22	75	57	116	77	115	84	151	...
2600	43	4071.74	1.61	-0.02	fmw	...	...	58	44	95	60	87	83	118	...
2600	43	4132.06	1.61	-0.67	ob	...	...	...	27	...	26	50	...	106	...
2600	43	4143.87	1.56	-0.51	ob	...	...	46	...	106	...	60	51	...	...
2600	42	4147.67	1.49	-2.10	fmw	...	...	...	...	...	...	...	...	...	58
2600	354	4181.76	2.83	-0.32	nk	...	...	...	...	35	...	...	...	...	114
2600	152	4187.80	2.43	-0.61	nk	...	...	...	...	34	...	...	...	...	...
2600	152	4198.31	2.40	-0.72	nk	...	...	...	...	...	20	...	...	...	...
2600	522	4199.10	3.05	0.14	nk	...	...	...	...	50	...	...	...	...	...
2600	42	4202.03	1.48	-0.71	fmw	...	...	37	...	79	46	67	65	118	...
2600	152	4210.35	2.48	-0.87	fmw	...	...	...	...	...	...	...	...	...	74
2600	693	4217.55	3.43	-0.48	ob	...	...	...	...	...	...	...	...	...	56
2600	152	4222.22	2.45	-0.97	fmw	...	...	...	...	...	...	...	...	...	85
2600	152	4235.94	2.43	-0.32	ob	...	...	...	...	53	27	39	37	57	158
2600	693	4238.82	3.40	-0.23	ob	...	...	...	...	...	...	...	...	...	78
2600	152	4250.13	2.47	-0.38	ob	...	...	...	...	...	...	30	29	...	...
2600	42	4250.79	1.56	-0.71	fmw	...	...	...	...	...	...	32	37	...	...
2600	152	4260.48	2.40	0.08	ob	...	...	35	30	85	44	60	53	79	...
2600	42	4271.76	1.48	-0.17	ob	...	10	...	54	...	...	...	...	...	...
2600	71	4282.41	2.18	-0.78	ob	...	...	...	...	48	...	...	...	...	...
2600	42	4325.77	1.61	0.01	ob	...	20	...	...	...	85	120	99	153	...
2600	41	4383.55	1.48	0.21	ob	...	24	...	...	145	102	149	115	191	...
2600	41	4404.75	1.56	-0.15	ob	...	...	...	39	119	65	91	82	128	...
2600	2	4427.31	0.05	-2.91	fmwy	...	...	...	...	...	...	...	...	...	90
2600	68	4447.72	2.22	-1.34	fmw	...	...	...	...	...	...	...	...	...	60
2600	68	4459.12	2.18	-1.33	ob	...	...	...	...	...	...	...	...	...	83
2600	350	4466.55	2.83	-0.59	fmw	...	...	...	...	...	...	...	...	...	68
2600	350	4476.02	2.85	-0.82	ob	...	...	...	...	...	...	...	...	...	61
2600	828	4484.23	3.60	-0.86	ob	...	...	...	...	...	...	...	...	...	15
2600	68	4494.57	2.20	-1.14	ob	...	...	...	...	...	...	...	...	...	108
2600	68	4528.62	2.18	-0.89	ob	...	...	...	...	58	...	...	...	...	...
2600	39	4531.15	1.48	-2.10	ob	...	...	...	...	...	...	...	...	...	53
2600	554	4736.78	3.21	-0.75	ob	...	...	...	...	28	...	...	...	...	65
2600	318	4890.76	2.88	-0.47	nk	...	...	...	...	...	...	...	...	35	...
2600	318	4891.50	2.85	-0.17	nk	...	...	...	...	68	...	...	...	48	...
2600	318	4903.32	2.88	-1.08	fmw	...	...	...	...	...	...	...	...	...	42
2600	318	4919.00	2.87	-0.34	fmw	...	...	...	...	34	...	32	21	45	112
2600	318	4920.51	2.83	0.07	fmw	...	...	34	23	68	...	61	39	77	...
2600	687	4966.10	3.33	-1.00	nk	...	...	...	...	...	...	...	...	...	50
2600	114	5049.83	2.28	-1.42	fmw	...	...	...	...	...	...	...	...	...	63
2600	1178	6024.07	4.55	-0.12	fmw	...	...	...	...	...	...	...	...	...	55
2601	3	3914.48	1.67	-4.10	nk	...	...	...	88	...	...	...	...	...	...
2601	3	3930.31	1.70	-4.03	nk	...	...	...	88	...	...	...	...	...	...
2601	126	4032.95	4.50	-2.70	nk	...	...	...	32	42	...	...	...	...	...
2601	172	4048.83	5.57	-2.15	nk	...	14	...	45	50	...	46	...	48	86

TABLE 11—*Continued*

Elem	Mult	Wavel	$\chi$	log gf	Comm	110	298	392	136	463	478	254	442	213	174
2601	212	4057.51	7.27	-1.55	nk	...	...	...	20	...	...	...	...	...	...
2601	28	4122.64	2.58	-3.38	nk	...	35	56	85	86	71	99	79	139	175
2601	22	4124.79	2.54	-4.20	nk	...	...	...	...	36	...	24	34	...	77
2601	27	4128.74	2.58	-3.77	fmw	...	14	...	...	...	60	...	...	...	...
2601	27	4173.45	2.58	-2.18	fmw	...	...	130	...	...	183	...	...	...	...
2601	28	4178.86	2.58	-2.48	fmw	78	81	...	...	...	188	...	...	...	...
2601	28	4258.16	2.70	-3.40	fmw	...	24	63	66	93	65	86	80	141	...
2601	27	4273.32	2.70	-3.34	fmw	...	30	...	70	88	72	88	90	124	142
2601	32	4278.13	2.69	-3.82	nk	...	11	...	32	...	...	28	...	67	...
2601	28	4296.57	2.70	-3.01	fmw	59	55	78	132	125	121	141	141	...	...
2601	27	4303.17	2.70	-2.49	fmw	93	81	...	...	...	182	...	...	...	...
2601	27	4351.76	2.70	-2.10	fmw	124	94	150	...	...	...	...	...	...	...
2601	213	4354.36	7.65	-1.34	nk	...	...	...	16	...	...	...	...	...	...
2601	28	4369.40	2.78	-3.67	fmw	...	...	...	46	63	38	55	49	77	126
2601	27	4385.38	2.78	-2.57	fmw	75	70	...	170	...	165	189	183	...	...
2601	32	4413.60	2.68	-3.74	fmw*	...	...	...	...	...	...	...	...	...	54
2601	27	4416.82	2.78	-2.60	fmw	75	...	...	...	...	...	...	...	...	...
2601	26	4461.43	2.58	-4.11	nk	...	...	...	...	...	...	...	...	...	119
2601	37	4472.92	2.84	-3.43	fmw	...	22	...	52	55	49	58	47	84	108
2601	37	4489.19	2.83	-2.97	fmw	40	46	...	125	118	113	125	128	178	...
2601	37	4491.40	2.86	-2.70	fmw	50	59	95	142	135	134	155	153	...	...
2601	38	4508.28	2.86	-2.21	fmw	104	86	118	...	...	193	...	...	...	...
2601	37	4515.34	2.84	-2.48	fmw	85	74	120	...	...	179	199	196	...	...
2601	37	4520.23	2.81	-2.60	fmw	68	70	108	178	152	160	191	188	...	...
2601	38	4522.63	2.84	-2.03	fmw	136	101	145	...	...	...	...	...	...	...
2601	37	4534.17	2.86	-3.47	fmw	37	...	...	...	...	...	...	...	...	...
2601	38	4541.52	2.86	-3.05	fmw	43	40	75	106	108	98	122	118	180	165
2601	37	4555.89	2.82	-2.29	fmw	96	81	...	...	...	193	...	...	...	...
2601	38	4576.33	2.84	-2.82	nk	46	44	74	108	111	94	...	...	174	168
2601	37	4582.84	2.84	-3.10	fmw	28	36	...	...	98	81	87	103	141	...
2601	38	4583.83	2.81	-2.02	fmw	...	128	...	...	...	...	...	...	...	...
2601	38	4620.51	2.83	-3.28	fmw	...	38	41	65	78	68	90	63	115	127
2601	37	4629.34	2.81	-2.37	fmw	91	82	130	...	...	189	...	...	...	...
2601	186	4635.33	5.96	-1.65	nk	41	30	...	55	37	43	48	41	70	...
2601	43	4656.97	2.89	-3.63	fmw	...	15	...	65	80	63	83	72	117	...
2601	44	4663.70	2.89	-4.26	nk	...	...	...	...	38	26	24	...	26	60
2601	37	4666.75	2.83	-3.33	fmw	21	27	51	68	70	62	80	60	115	135
2601	25	4670.17	2.58	-4.10	nk	...	...	...	...	...	40	...	...	...	...
2601	43	4731.44	2.89	-3.36	fmw	33	34	63	81	90	83	110	92	136	145
2601	36	4893.78	2.83	-4.45	fmw	...	...	...	...	...	...	...	...	...	34
2601	42	4923.92	2.89	-1.32	fmw	...	152	...	...	...	...	...	...	...	...
2601	36	4993.36	2.81	-3.65	fmw	...	...	16	...	52	...	39	51	65	90
2601	42	5018.43	2.89	-1.22	fmw	...	154	...	...	...	...	...	...	...	...
2601	35	5146.12	2.83	-3.91	nk	...	...	...	...	39	...	...	...	...	57
2601	35	5150.93	2.86	-4.45	nk	...	...	...	...	...	...	...	...	...	61
2601	42	5169.03	2.89	-0.87	fmw	...	175	...	...	...	...	...	...	...	...
2601	49	5197.57	3.23	-2.10	fmw	87	76	112	...	...	164	...	194	...	...
2601	49	5234.62	3.22	-2.05	fmw	...	...	...	...	...	171	...	...	...	...

TABLE 11—*Continued*

Elem	Mult	Wavel	$\chi$	log gf	Comm	110	298	392	136	463	478	254	442	213	174
2601	46	5991.38	3.15	-3.59	fmw*	...	...	...	12	41	...	...	31	...	88
2601	200	6103.54	6.22	-2.17	nk	...	...	...	25	...	...	...	...	...	...
2601	74	6147.74	3.89	-2.46	fmwy*	22	37	...	57	80	62	65	69	78	100
2601	74	6149.24	3.89	-2.77	fmw*	28	28	...	50	63	52	50	61	81	95
2601	200	6175.16	6.22	-1.98	nk	...	...	...	25	...	...	...	...	...	...
2601	163	6179.38	5.57	-2.66	fmw*	...	...	...	18	...	...	...	...	...	...
2601	74	6238.38	3.89	-2.48	fmw*	...	...	...	65	...	...	57	...	...	...
2601	74	6247.56	3.89	-2.36	fmw*	...	...	70	115	...	113	129	114	161	159
2601	199	6331.97	6.22	-1.98	nk	...	...	...	26	31	...	...	...	...	...
2601	40	6416.08	2.89	-3.15	fmw*	...	...	...	...	...	65	...	...	...	...
2601	74	6416.91	3.89	-2.55	fmw*	49	...	...	45	60	53	...	64	...	116
2601	40	6432.65	2.89	-3.54	fmw*	...	...	...	...	51	36	...	36	...	...
2601	199	6446.43	6.22	-2.01	fmw*	...	...	...	30	...	...	...	...	...	...
2601	74	6456.38	3.90	-2.15	fmw*	77	70	...	150	...	142	...	...	...	...
2601	73	7307.97	3.89	-3.02	nk	...	...	...	...	...	...	...	...	...	53
2601	73	7449.34	3.89	-3.31	nk	...	...	...	...	...	27	...	...	29	72
2601	73	7462.38	3.89	-2.73	nk	...	...	...	35	90	37	...	66	63	110
3801	1	4077.71	0.00	0.15	wm	...	...	58	43	110	59	98	81	175	...
3801	1	4215.52	0.00	-0.16	wm	...	...	46	35	108	41	72	59	122	...
4001	54	4024.45	1.00	-0.97	nk	...	32	...	...	...	...	...	...	...	...
4001	41	4149.22	0.80	-0.03	nk	...	...	...	17	46	27	36	43	68	138
4001	40	4496.96	0.71	-0.81	nk	...	...	...	...	...	...	...	...	...	49
5601	1	4934.09	0.00	-0.16	nk	...	...	...	...	53	19	23	13	54	196
5601	2	6496.90	0.60	-0.38	nk	...	...	...	...	...	...	...	...	...	119

NOTE.— bghl = Biémont et al. 1981, mfw = Martin et al. 1988, fmw = Fuhr et al. 1988, fmwy = Fuhr et al. 1981, ob = O’Brian et al. 1991, op = Opacity Project (Hibbert et al. 1991), nk = new Kurucz (1990), sl = Sigut & Landstreet 1990, wm = Wiese & Martin 1980, wsm = Wiese et al. 1969, zhu = Zhu et al. 1989. Some Fe II log(gf) values have been marked with a “\*”. These have been determined from analyses of the Sun, adopting  $\log(\text{Fe})+12=7.66$ . This Fe value is 0.15 dex larger than the meteoritic abundance adopted here, and thus, those Fe II oscillator strengths have been raised by 0.15 dex.